nature mental health

Article

https://doi.org/10.1038/s44220-024-00309-y

A mega-analysis of functional connectivity and network abnormalities in youth depression

Received: 2 February 2024

Accepted: 13 August 2024

Published online: 23 September 2024

Check for updates

Nga Yan Tse[1], Aswin Ratheesh[2,3,4], Ye Ella Tian[1], Colm G. Connolly[5], Christopher G. Davey[6], Saampras Ganesan[1,7,8], Ian H. Gotlib[9], Ben J. Harrison[6], Laura K. M. Han[2,3], Tiffany C. Ho[10], Alec J. Jamieson[6], Jaclyn S. Kirshenbaum[11,12], Yong Liu[13], Xiaohong Ma[14], Amar Ojha[15,16], Jiang Qiu[17,18], Matthew D. Sacchet[19], Lianne Schmaal[2,3], Alan N. Simmons[20,21], John Suckling[22,23], Dongtao Wei[17,18], Xiao Yang[14], Tony T. Yang[24], Robin F. H. Cash[1,7,25] & Andrew Zalesky[1,7,25]

Major depressive disorder (MDD) represents the leading cause of mental health disability for young people worldwide but remains poorly understood. Previous neuroimaging research has indicated alterations in the connectivity of brain circuitry in youth MDD; however, findings have been inconsistent. This may relate to limitations in sample size and sample and methodological heterogeneity. In an effort to delineate robust neurobiological markers of youth MDD, we conducted a data-driven, connectome-wide mega-analysis of resting-state functional connectivity in 810 young individuals across 7 independent cohorts with a cross-sectional and case-control design. Compared with healthy comparison individuals ($n = 370$), youth MDD ($n = 440$) was associated with significant alterations in connectivity of densely connected brain areas (hubs), anchored in the default mode and dorsal and ventral attention networks. Critically, functional connectivity within these networks was significantly associated with depression symptom severity ($r = -0.46$ for hypoconnected regions and $r = 0.53$ for hyperconnected regions; both P values < 0.001), indicating the clinical relevance of functional connectivity alterations. Further, machine-learning analyses demonstrated that individual diagnostic status (AUC = 73.1%) and clinical severity ($r = 0.14$, $P = 0.008$) could be predicted on the basis of functional connectivity alone in unseen data using leave-one-site-out cross-validation. Together, our work represents an important first step toward robust characterization of the neurobiological basis of youth depression. We demonstrate the clinical relevance of brain connectivity in youth depression and highlight a critical role of functional hub regions, especially those localized to the default mode and dorsal and ventral attention networks in youth MDD.

A full list of affiliations appears at the end of the paper. e-mail: azalesky@unimelb.edu.au

Major depressive disorder (MDD) has a lifetime prevalence of 11.1–14.6% (refs. 1,2) and represents the leading cause of disability due to mental health conditions for young people aged 10–24 years worldwide[3,4]. Early onset is associated with pervasive functional impairments across academic and occupational domains and poorer clinical outcomes[5–9]. Despite the high prevalence and poor prognosis, the neurobiological basis of youth MDD remains under-characterized.

Functional neuroimaging can delineate the neural substrates of psychiatric, cognitive and neurological disorders and potentially provide targets for treatment[10–16]. However, findings in youth MDD have remained inconsistent. A recent meta-analysis of task-based functional magnetic resonance imaging (fMRI) studies in youth MDD reported an absence of significant brain activation/deactivation clusters after combining attention, emotion, reward processing and executive function tasks[17]. Likewise, a recent meta-analysis of resting-state fMRI connectivity did not observe significant spatial convergence of past seed-based functional connectivity findings in youth MDD[18]. The majority of past empirical studies are limited by small sample sizes, which is further compounded by substantial inter-study variation. This includes heterogeneity in cohort characteristics as well as methodological factors across acquisition, pre-processing and analytical approaches[18], thus leading to an inconclusive picture of the neurobiological mechanism of youth MDD. More generally, inconsistencies and lack of generalizability across independent neuroimaging studies have raised concerns about the neurobiological, clinical and translational value of neuroimaging findings[19–21].

One approach to address some of these limitations is through mega-analyses. This involves collation and analysis of multiple independent cohort datasets, boosting statistical power and increasing the site-independent generalizability of research findings[22–24]. Reproducibility and generalizability can be further enhanced by leveraging standardized and openly available MRI pre-processing pipelines that are based largely on field expert consensus. This approach additionally avoids the confounding impact of heterogeneous MRI pre-processing and analysis pipelines inherent to meta-analyses[25]. Critically, the increase in statistical power allows for impartial data-driven analyses across the whole brain, avoiding the potential perpetuation of prior notions around circumscribed sources of neurobiological dysfunction, which otherwise represents a necessary starting point for seed-based analyses of smaller datasets. Single-site studies may train and evaluate predictive models using subsets of the same cohort, but it typically remains unclear whether these models will generalize to external datasets[26,27]. By contrast, multi-site studies enable site-independent reproducible and generalizable functional connectivity features to be established. These advantages are central to clinical translation.

Here we compiled a large multi-site resting-state fMRI dataset acquired in young individuals with MDD and healthy comparison individuals from seven existing cohorts scanned at six sites across four countries (n = 810 youth participants). Standardized imaging pre-processing, quality control and harmonization were completed for all fMRI data, and functional brain networks (connectomes) were mapped for each individual. Using these standardized connectomes, we aimed to robustly (1) characterize disruptions in functional connectivity and distributed brain networks in youth MDD using impartial, whole-brain statistical inference; (2) identify connections that are consistently associated with depression symptom severity; and (3) apply machine-learning predictive models to parse connectivity biomarkers that are most robust to inter-individual and inter-site variability.

Results

We conducted the largest mega-analysis by sample size of resting-state functional connectivity in youth MDD. A total of 27 datasets were identified, and 6 groups agreed to provide the required neuroimaging data. Beyond non-response, reasons for nonparticipation included departmental- and ethics-related restrictions on data sharing.

Table 1 | Demographic and head motion variables for MDD and HC groups

	MDD(n=440)	HC(n=370)	t value	d.f.	P value
Age [range]	18.39 (3.12) [12.00–25.60]	20.12 (3.24) [12.14–25.89]	7.734	808	<0.001
Sex (F/M)	288/152	240/130	0.031[a]	2	0.861
Head motion					
Mean FD	0.11 (0.04)	0.10 (0.04)	0.328	808	0.743
Mean DVARS	18.27 (4.72)	17.89 (4.79)	1.151	808	0.250
Mean RMSD	0.06 (0.02)	0.06 (0.02)	−0.615	808	0.539
Mean outlier volume (%)	3.06 (3.30)	2.81 (3.51)	−1.028	808	0.304

Values given as mean (s.d.); t values are two-sided independent sample t-statistic values. DVARS, the derivative of root mean square variance over voxels; FD, framewise displacement; HC, healthy comparison individuals; outlier volume, number of volumes with standardized DVARS value > 1.5/FD > 0.5mm; RMSD, root mean square deviation (a quantification of the estimated relative (frame-to-frame) bulk head motion). [a]Chi-square value.

The final sample following quality control comprised 440 youths with MDD and 370 healthy comparison individuals aged between 12 and 25 years (Table 1). Detailed information regarding clinical characteristics, diagnostic assessment tools and inclusion and exclusion criteria can be found in Table 2 and Supplementary Tables 1 and 2, respectively. Our study design included four core components: (1) standardized fMRI pre-processing, quality control, harmonization and mapping of whole-brain functional networks; (2) whole-brain-based inference to identify functional connections that differ in connectivity strength between young individuals with MDD and young healthy comparison individuals, as well as those that associate with measures of depression symptom severity; (3) inference to identify canonical functional networks for which within- and between-network connectivity associates with symptom severity; and (4) predictive modeling of individual diagnostic status and symptom severity using leave-one-site-out cross-validation (see Fig. 1 for a schematic overview).

Functional connectivity changes in youth MDD

Leveraging an impartial, whole-brain approach termed network-based statistics (NBS)[28] and controlling for age and sex, we found that youth MDD (n = 440) was associated with distinct patterns of hyper- and hypoconnectivity relative to the healthy comparison group (n = 370; P = 0.012 and 0.005, respectively). According to the total number of significant connections linked with each region, increased connectivity was localized to the inferior and superior parietal regions and the anterior insula, as well as the somatosensory, auditory and visual regions and the medial thalamus (Fig. 2a). The magnitude of difference represented a medium effect size as indicated by a Cohen's d of −0.45 (Fig. 2c). To provide additional insight into the contributing functional networks, regions of each pair of significant connections were assigned to their respective canonical networks (Supplementary Section 1.1). This revealed that increased connectivity between the dorsal attention network (DAN) and several other networks, including the salience/ventral attentional network (VAN), somatomotor network (SMN) and central executive network (CEN), was evident in MDD. Hyperconnectivity within the VAN was additionally observed (Fig. 2b). Overall, there is a predominant disruption to the attentional systems in MDD-related hyperconnectivity compared with healthy comparison individuals.

The MDD group also demonstrated significantly reduced connectivity involving many core default mode network (DMN) regions, including the medial prefrontal cortex (mPFC), rostral anterior cingulate cortex (ACC)/subgenual cingulate cortex (SGC), posterior cingulate cortex (PCC) and superior frontal gyrus. The orbitofrontal cortex and the superior parietal, temporal pole and somatosensory regions

https://doi.org/10.1038/s44220-024-00309-y

Table 2 | Differences in demographic and clinical variables within the MDD group by site

	Site 1 Melbourne 1 (YoDA-C) (*n*=123)	Site 2 Melbourne 2 (*n*=45)	Site 3 TAD+ TIGER (*n*=106)	Site 4 MR-IMPACT (*n*=63)	Site 5 China (*n*=54)	Site 6 UCSF (*n*=49)	d.f. (group, total)	*F* value	*P* value	Bonferroni-corrected post hoc comparison
Age	19.78 (2.79)	19.40 (2.43)	17.38 (2.90)	15.72 (1.23)	21.35 (2.96)	16.31 (1.37)	5, 439	48.450	<0.001	Sites 1 and 2 > Sites 3, 4, 6 Site 3 > Site 4 Site 5 > Sites 1, 2, 3, 4, 6
Sex (F/M)	73/50	28/17	74/32	53/10	28/26	32/17	5	17.259[a]	0.004	—
Ethnicity (white/African/ Asian/multiracial/ other/missing)	(99/1/20/0/3/0)	(34/0/8/1/2/0)	(50/4/16/8/10/18)	(57/0/0/4/2/0)	(0/0/54/0/0/0)	(8/4/1/15/21/0)	—	—	—	—
Diagnosis tool	SCID	SCID	K-SADS-PL	K-SADS-PL	SCID	K-SADS-PL	—	—	—	—
RCT (Y/N)	Y	N	N	Y	N	N	—	—	—	—
RCT Interventions	CBT+ fluoxetine/ placebo	—	—	CBT/STPP/ SCC	—	—	—	—	—	—
Depression symptom measure	MADRS	MADRS	CDRS-R (*n*=88)/ BDI-II (*n*=18)	SMFQ	HAMD-17	MADRS	—	—	—	—
MADRS band score[b]	14.50 (2.42)	11.82 (3.18)	9.31 (2.86)	N/A	10.67 (3.06)	11.21 (3.74)	4, 347	44.112	<0.001	Site 1 > Sites 2, 3, 5, 6 Sites 2 and 5 > Site 3
MADRS raw/ converted score	33.16 (5.50)	26.73 (7.66)	20.49 (7.08)[c]	17.87 (4.78)[d]	24.07 (7.53)[c]	25.06 (9.22)	—-	—	—	—
Antidepressant history (Y/N)	31/90	8/37	N/A	N/A	19/25	10/38	—	—	—	—

Values are given as mean (s.d.). Participant ethnicity was identified on the basis of self-report. *F* values are one-way independent analysis of variance *F* values (two-sided).CBT, cognitive–behavioral therapy; F, female; K-SADS-PL, Kiddie Schedule for Affective Disorders and Schizophrenia–Present and Lifetime; M, male; N, no; N/A, information not available; RCT, randomized controlled trial; SCC, specialist clinical care; SCID, Structured Clinical Interview for *Diagnostic and Statistical Manual of Mental Disorders* 4th Edition[117] Axis I Disorders; SMFQ, Short Mood and Feeling Questionnaire; STPP, short-term psychoanalytic psychotherapy; Y, yes. [a]Chi-square value. [b]Refer to Supplementary Table 3 for calculation of MADRS band scores. [c]Converted from CDRS-R and HAMD-17 for Sites 3 (*n*=88) and 5, respectively. [d]SMFQ raw score.

as well as the insula and thalamus also demonstrated hypoconnectivity (Fig. 2d). The overall effect size was medium ($d = 0.42$; Fig. 2f). When hypoconnected regions were spatially assigned to their respective canonical networks, the DMN showed reduced connectivity with the DAN and VAN (Fig. 2e). Within-limbic and limbic–VAN hypoconnectivities were also observed (Fig. 2e). In summary, MDD-specific hypoconnectivity spanned a distributed network of regions, implicating primarily the default mode as well as attentional and limbic networks.

In addition, a significant sex-by-diagnosis interaction was evident. Connectivity in the visual, cuneus, somatosensory, premotor and dorsal mPFC as well as the anterior thalamus was lower in female MDD compared with male MDD individuals (Supplementary Fig. 1). Conversely, male MDD participants demonstrated lower connectivity lateralized to right visual, somatosensory, posterior parietal and retrosplenial cortex relative to female counterparts (Supplementary Fig. 2). No significant effects were detected for age-by-diagnosis interaction.

Stratifying the clinical group by the presence of any previous antidepressant treatment history implicated the thalamus and the striatum. In those with a history of pharmacological intervention, these subcortical structures showed increased connectivity with predominantly the SMN and DAN (Supplementary Fig. 3i), as well as decreased connectivity with the DMN and CEN (Supplementary Fig. 3ii).

Connectivity and network changes in depression severity

Next we investigated whether functional connectivity was associated with depression symptom severity in the subset of 348 MDD individuals with either raw or converted Montgomery–Asberg Depression Rating Scale (MADRS) scores. We used psychometrically established conversion scales from the Children's Depressive Rating Scale–Revised (CDRS-R)[29] or the Hamilton Depression Rating Scale-17 item (HAMD-17)[30]. Considering the significant site difference in MADRS (Table 2), site effect was regressed from MADRS scores before further analysis (Methods). Controlling for age and sex, NBS revealed that higher functional connectivity involving the intraparietal sulcus, superior parietal, retrosplenial and motor regions, as well as the insula, was significantly associated with higher depression severity as measured by the total MADRS score ($P = 4.14 \times 10^{-26}$, $r = 0.53$; Fig. 3a,e). At the network level, these connections localized predominantly to the attentional and visual systems, including the dorsal and ventral attentional and visual networks (Fig. 3b). Subcortical structures, including the putamen and inferior thalamus, were also implicated. Together, these findings indicate that greater symptom severity was associated predominantly with attentional and sensory network hyperconnectivity in youth MDD.

Greater symptom severity was also associated with lower connectivity involving the mPFC, precuneus, angular gyrus, supplementary motor area and superior and inferior parietal areas, as well as the putamen ($P = 1.57 \times 10^{-19}$; $r = -0.46$; Fig. 3c,e). At the network level, the DMN similarly demonstrated widespread hypoconnectivity with multiple networks spanning the DAN, VAN and CEN (Fig. 3d). These findings indicate that DMN- and attentional network-centered hypoconnectivity, observed in our earlier analysis of functional connectivity abnormalities in youth MDD, also relate to symptom severity.

We next sought to quantitatively identify networks that most consistently contribute to depression severity. Specifically, we computed inter- as well as intra-network connectivity strength within and between each pair of the seven canonical networks, averaged across all constituent connections of each network (Supplementary Section 1.2). This analysis was constrained to cortical regions. After controlling for age and sex across all network pairs and using site-regressed MADRS scores, greater depression severity was associated with lower connectivity between the DMN and DAN ($r = -0.15$, $P = 0.007$) and VAN ($r = -0.16$, $P = 0.003$) and CEN ($r = -0.11$, $P = 0.034$), as well as between

https://doi.org/10.1038/s44220-024-00309-y

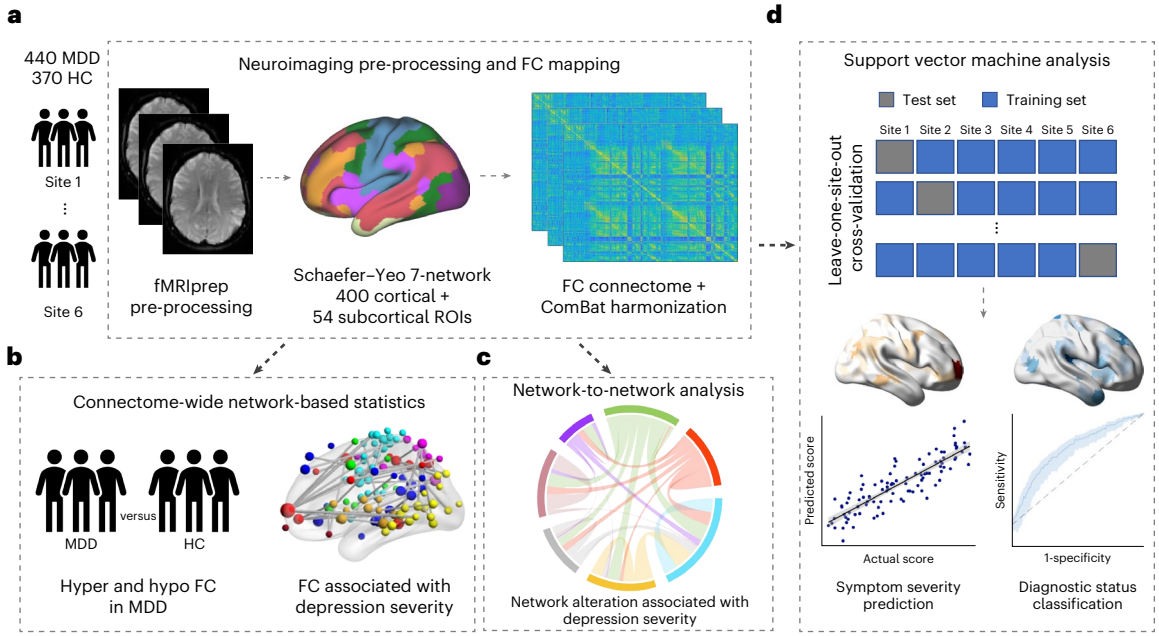

Fig. 1 | Mega-analysis design and workflows. Whole-brain characterization of functional connectivity in youths with MDD. **a**–**c**, After image pre-processing and functional connectivity mapping (**a**), mega-analyses of between-group and symptom severity-related connectivity differences were conducted at the scale of functional connections (**b**) and canonical networks (**c**). **d**, Support vector machines with leave-one-site-out cross-validation were applied to generate and evaluate predictive models of diagnostic status and symptom severity. FC, functional connectivity; ROI, region of interest.

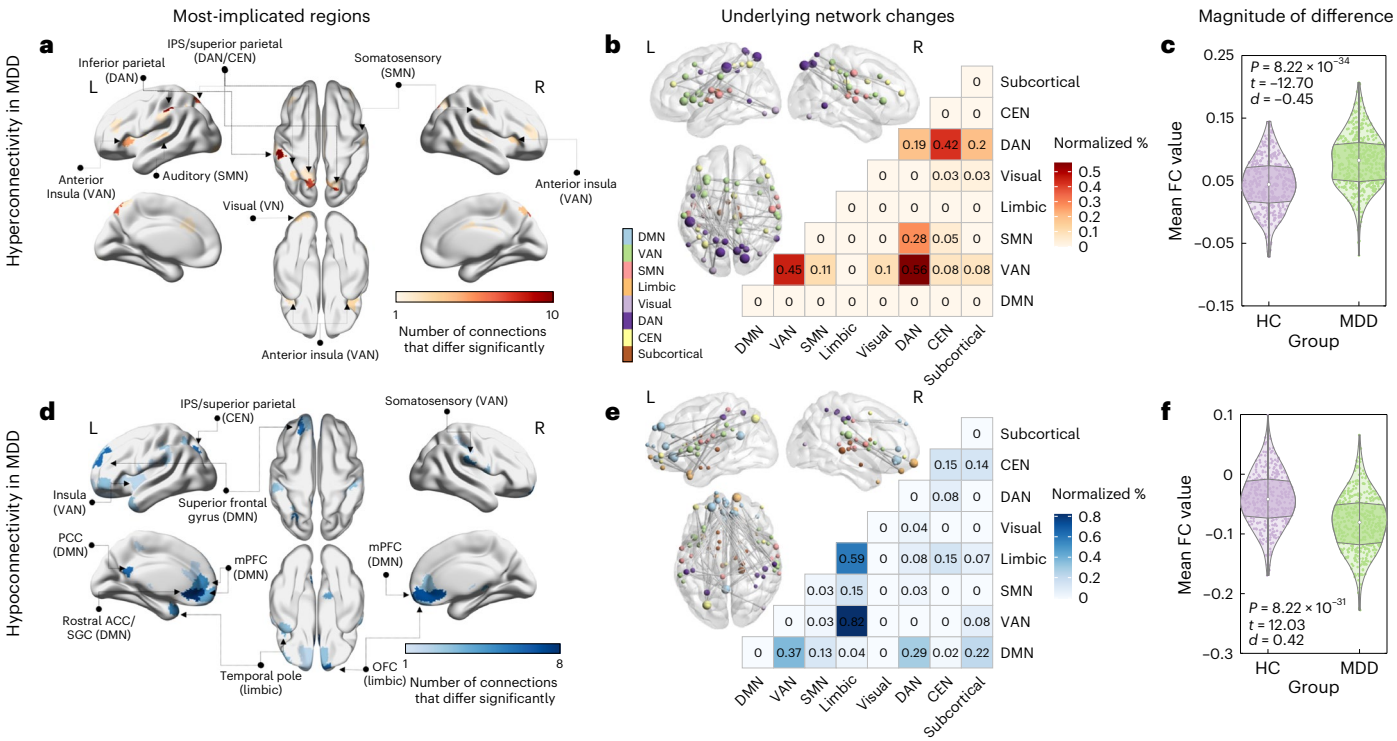

Fig. 2 | Functional connectivity changes in youth MDD compared with HC individuals controlling for age and sex. a, Cortical renderings show regions significantly associated with higher functional connectivity in youth MDD. Colors represent the total number of connections that differ significantly between groups. **b**, Networks showing connections with significantly higher connectivity strength in youth MDD. Nodes are colored according to seven canonical functional networks and sized proportionally to the total number of significant connections linked with each node. Matrix displays proportion of connections with significantly higher connectivity strength between pairs of canonical networks, normalized by the total number of possible connections within or between each pair of networks. **c**, Significantly higher mean connectivity values of all significant hyperconnections (as shown in **b**) in MDD ($n = 440$; mean = 0.08; s.d. = 0.04) compared with the HC group ($n = 370$; mean = 0.04; s.d. = 0.04) on two-sided independent sample t test. **d**–**f**, Same as **a**–**c** but for lower functional connectivity in the MDD group ($n = 440$; mean = −0.08; s.d. = 0.05) relative to the HC group ($n = 370$; mean = −0.04; s.d. = 0.05) on two-sided independent sample t test. IPS, intraparietal sulcus; L, left; OFC, orbitofrontal cortex; R, right. Cortical renderings were generated using the BrainNet Viewer toolbox[135].

https://doi.org/10.1038/s44220-024-00309-y

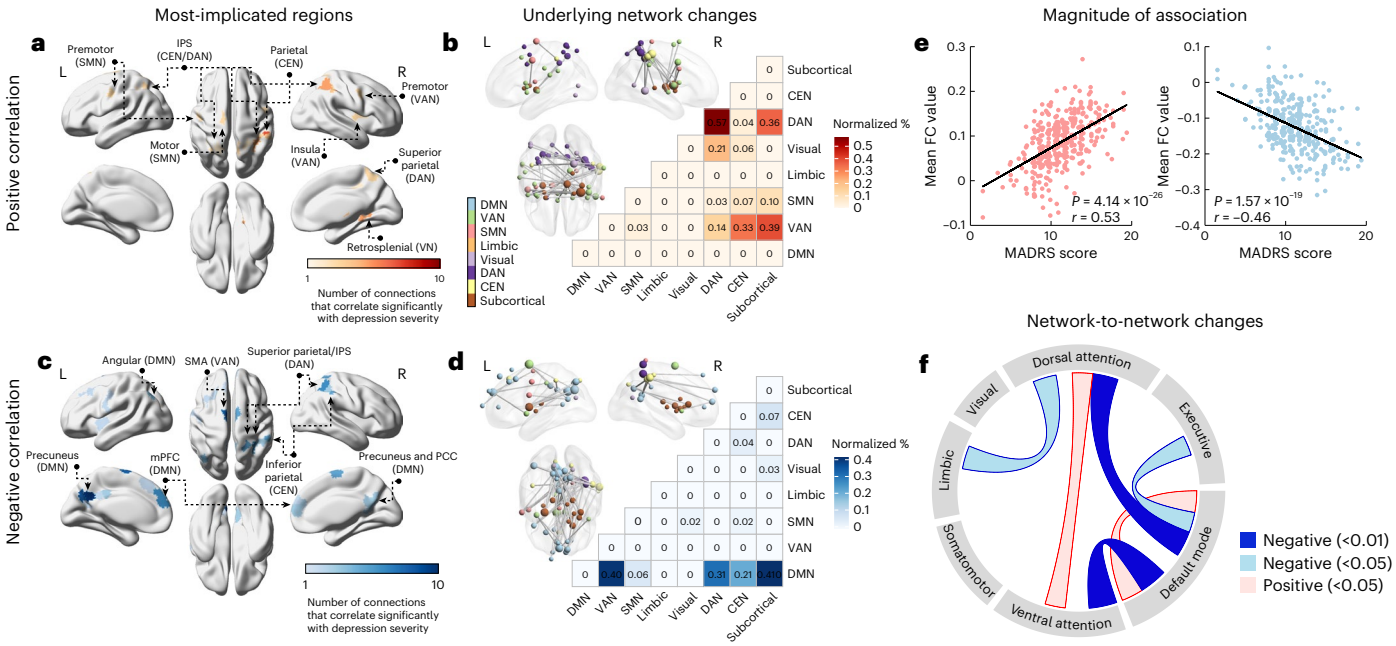

Fig. 3 | Depression symptom severity-related functional connectivity and network changes controlling for age and sex. a, Regions significantly associated with higher depression severity as reflected by a positive association with higher site-regressed total MADRS scores. Colors depict the total number of connections that correlate significantly with depression severity. **b**, Networks containing connections significantly associated with higher site-regressed total MADRS scores. Nodes are colored according to seven canonical functional networks. Node size is proportional to the total number of significant connections linked with each node. Matrix displays proportion of connections with significant association with higher site-regressed total MADRS scores between pairs of canonical networks, normalized by the total number of possible connections within or between each pair of networks. **c**,**d**, Same as **a**,**b** but for negative association with site-regressed total MADRS scores. **e**, The magnitude of correlations between mean connectivity strength of all significant positive and negative connections and site-regressed MADRS scores, respectively, as determined by Pearson correlation coefficient. A two-sided *P* value was used to determine significance. **f**, Significant correlation between network connectivity and depression severity (site-regressed MADRS scores). Line width reflects the size of the correlation coefficient. Cortical renderings were generated using the BrainNet Viewer toolbox[135].

the limbic and dorsal attention networks ($r = -0.13$; $P = 0.013$; Fig. 3f). Conversely, heightened intra-DMN ($r = 0.12$, $P = 0.022$) and DAN–VAN ($r = 0.12$, $P = 0.032$) connectivities were positively associated with more severe depression symptoms (Fig. 3f). Together, these results provide convergent evidence of strong default mode and attentional network involvement as a broader functional network signature of youth MDD symptom severity.

The effect of hubness. Several of the regions implicated in the preceding are considered brain hubs, such as the mPFC, ACC, PCC, precuneus, lateral parietal, visual and insular regions (see reviews in refs. 31–33). Dysfunctional hub connectivity is implicated in disorders characterized by an early onset, including autism spectrum disorder, attention deficit hyperactivity disorder and schizophrenia[31,32]. As such, we further investigated this observation and assessed the hubness of each node, determined by a region's total connectivity strength to all other regions (Supplementary Section 2). This revealed that greater levels of hubness were significantly associated with a greater magnitude of between-group differences ($r = 0.11$; $P \leq 0.023$; Supplementary Fig. 4) as well as symptom severity correlations ($r = 0.24$–0.25; $P < 0.001$; Supplementary Fig. 5), providing additional insight into the contribution of hub regions to youth MDD.

The effect of global signal regression and head motion. Supplementary analyses (Supplementary Section 3) demonstrated that the inclusion of an additional head motion covariate (Supplementary Figs. 6 and 7), the adoption of a more stringent head motion exclusion criteria (Supplementary Fig. 8) and the absence of global signal regression (Supplementary Fig. 9) did not alter the overall pattern of findings across NBS between-group and correlational analyses.

Predicting depression status and severity in unseen data

Using leave-one-site-out cross-validation, we established models to predict individual-level diagnostic status and symptom severity on the basis of patterns of functional connectivity. Principal components analysis (PCA) was performed on the training data to reduce the dimensionality of the functional connectivity matrices and alleviate the risk of overfitting. Support vector machines were trained on the resulting principal component scores. The test data were projected on the principal components, and resulting scores were used to derive predictions (Methods). PCA was performed separately for each training fold.

Validating the model performance in the held-out site, we showed that youth with MDD ($n = 440$) can be distinguished from healthy comparison individuals ($n = 370$) with an average accuracy of 73% (an overall area under the curve (AUC) of receiver operating characteristic (ROC) of 73.1% across all held-out test sets; Fig. 4a). Individual test set (unseen site) prediction accuracy ranged from 50.9% to 73.3%. We found that diagnostic prediction models trained on age and sex (overall AUC = 53.5%) or age alone (overall AUC = 53.7%) did not exceed chance-level performance. This indicates that diagnostic status did not show a disproportionate representation across specific age groups or sex.

Models integrating functional connectivity strengths could significantly predict symptom severity ($r = 0.14$, $P = 0.008$, $n = 348$; Fig. 4b), although predictions were weaker and not statistically significant within individual sites (with individual r values ranging from 0.13 to 0.20 except for site 2; Supplementary Fig. 10), most likely due to the reduced sample sizes.

To delineate the functional connections that were most important to our predictive models, the principal component feature weights were projected to the space of the functional connectivity matrix, and the Haufe transform[34] was then applied to the projected feature weights

https://doi.org/10.1038/s44220-024-00309-y

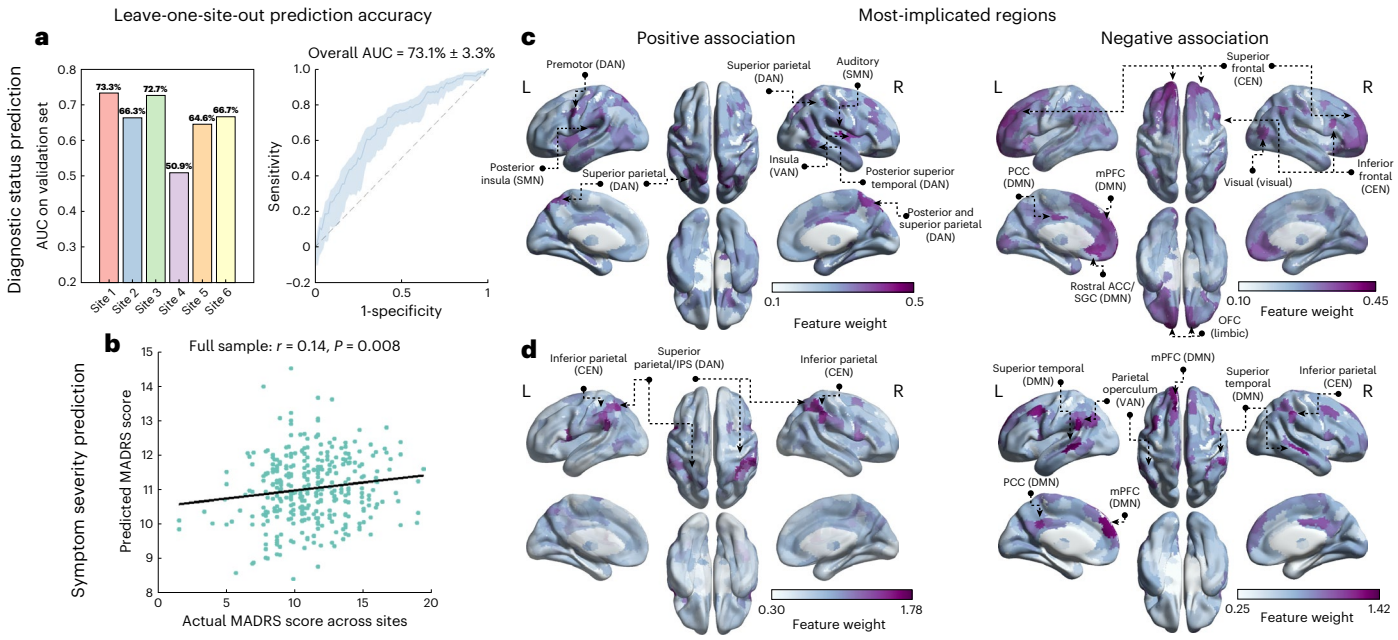

Fig. 4 | Predictive models of diagnostic status (depression or HC individual) and depression severity. a, Accuracy of the SVM classifier in distinguishing MDD diagnostic status. Left bar plot indicates AUC of ROC for each leave-one-site-out cross-validation model; right line graph reflects overall AUC derived from the entire sample with the shaded area denoting 95% confidence intervals for the ROC curve (determined using 1,000 bootstrap samples). **b**, Symptom severity prediction accuracy quantified by Pearson correlation coefficient between actual and predicted site-regressed MADRS scores for the entire sample across all leave-one-site-out cross-validation models. A two-sided *P* value was used to determine significance. **c**,**d**, Brain regions contributing the most to distinguishing young individuals with MDD from healthy comparison individuals (**c**) and symptom severity prediction (**d**) across the directions of positive and negative association. Colormap represents feature weights as indicated by the associated mean Haufe transformed beta values across leave-one-site-out cross-validation models averaged across 100 iterations. Cortical renderings were generated using the BrainNet Viewer toolbox[135].

to enable their interpretation. Overall, prediction of diagnostic status and symptom severity was found to be most strongly driven by positive connectivity of DAN regions with the highest consistency observed for the superior parietal cortex (Fig. 4c,d). By contrast, the DMN regions were highlighted in negative connectivity with the mPFC (including rostral ACC/SGC) and PCC being most consistently implicated (Fig. 4c,d). Averaged network-level feature weights also implicated the DMN and DAN as the most salient networks in negative and positive association, respectively, for both classification (Supplementary Fig. 11) and regression (Supplementary Fig. 12). Overall, our machine-learning analyses highlighted connectivity within largely the same set of regions and networks as our previous NBS analyses, supporting the central importance of core DAN (superior parietal cortex) and DMN regions (mPFC, SGC and PCC).

Collectively, our findings indicate that youth MDD is associated with robust changes in functional connectivity anchored to core components of the default mode and attentional networks. These regions tended to have a higher level of hubness and demonstrated significant predictive accuracy on independent machine-learning analyses.

Discussion

This work represents the largest mega-analysis of resting-state functional connectivity changes in youth MDD to date. Our findings indicate robust alterations in connectivity anchored in the default mode and dorsal and ventral attention networks. Dysfunctional connectivity localized to hub regions within these networks, extending on earlier studies reporting hub involvement in early psychopathology development[31,32]. We also established machine-learning models that predicted diagnostic status and depression severity with significant accuracy, implicating predominantly the same set of regions and networks. Together, the consensus across analyses underscores the critical involvement of networks that pertain to introspective and attentional processing in youth MDD.

Distributed network involvement in youth MDD

Controlling for age and sex, our analyses consistently implicated core nodes of the DMN, particularly the rostral ACC/SGC, mPFC, PCC and precuneus. In addition, altered connectivity of individual components of the dorsal and ventral attentional networks tended to emerge in youth MDD. These regions included the insula, striatum and intraparietal sulcus/superior parietal cortex. Our findings expand on previous resting-state fMRI studies in youth MDD that have often been constrained to specific regions or connections of interest due to limitations in sample size and statistical power. Interestingly, our observations converge with past studies that have typically included age and sex as covariates, which also demonstrated functional topological alterations anchoring in the default mode and attentional networks[18,35]. As such, these network alterations may represent universal biomarkers of youth MDD beyond age and sex.

The observed regions and networks of dysfunction are also well aligned with systematic review and meta-analytical findings in adult MDD across resting-state and task-based functional alterations[15,36–39]. An exception is the CEN, which did not emerge as a core component in our analyses. Changes in CEN connectivity are widely implicated in adult MDD[15,36–39] and more prominent in late-onset than early/mixed-onset MDD studies[40]. The absence of CEN involvement in our findings may reflect the higher neurodevelopmental variability associated with the protracted maturation of frontal systems during adolescence and early adulthood[41,42]. However, the meta-analytical observation of greater frontal involvement in studies with more patients on antidepressants also necessitates consideration of the potential confounding influence of treatment effects, especially since the current sample is predominantly medication-naïve. In addition, this discrepancy may stem from the investigation of spatially targeted hypotheses (for example, the use of region-of-interest approaches) in previous adult MDD work. Nonetheless, a substantial overlap was evident, with disruptions to default mode and attentional system connectivity being common to

both youth and adult MDD. This suggests a potential trajectory of disruption that may begin in youth and remains relatively constrained to a common set of processes and brain systems across the illness course.

A significant sex-by-diagnosis interaction implicated select regions of the visual, somatosensory, motor and thalamic regions. The age-by-diagnosis interaction was not significant. Given the lack of previous large-scale, connectome-wide work on sex effects in youth MDD, the specific sex-by-diagnosis interaction effects we observed here should be interpreted with caution. Although based on evidence from past work that has comprehensively examined resting-state fMRI connectivity differences between sex across the whole brain, the implicated regions, particularly the occipital and thalamic connectivity, have consistently emerged in whole-brain machine learning to be the most discriminative regions in the classification of sex in healthy young adults[43,44]. While these studies were conducted in healthy young adults, the convergence with our findings suggests that these regions may merit further investigation in future studies focusing on youth MDD.

When stratifying the clinical sample broadly by the presence of antidepressant medication history, alterations were most prominent between the subcortical regions (the thalamus and striatum) and the DMN and SMN. Notwithstanding the absence of an active experimental condition and the reduced sample size available for this analysis, our observation of reduced subcortex–DMN connectivity in patients with a previous medication history may be reminiscent of the normalization of DMN hyperconnectivity reported with remission in adult MDD following antidepressant or noninvasive brain stimulation treatment[45–47]. Interestingly, the thalamus has also been implicated as one of the key subcortical structures in antidepressant treatment outcome[46]. However, considerable variability is likely present within this subsample as influential confounds such as dose, duration and number of previous antidepressant trials were unavailable and thus not considered in the analysis. As such, these observations warrant cautious interpretation. Future studies equipped with comprehensive treatment information will be better positioned to facilitate a more nuanced delineation.

Hub connectivity changes and vulnerability

We found that connectivity changes associated with youth MDD converged on topologically central brain nodes (hub regions). Strikingly, almost all identified regions in our findings have been previously implicated as rich-club nodes (densely interconnected hub regions facilitating global communication and integrative processing), encompassing the mPFC, ACC, PCC, precuneus, lateral parietal and insular regions (see reviews in refs. 31–33). In alignment with our findings, abnormal volume in the mPFC, rostral ACC and insula has been shown to demonstrate the highest consistency in predicting onset of MDD across community and at-risk samples of children and adolescents (see review in ref. 48), underscoring their critical involvement in early MDD development.

Hub regions are highly connected regions, often considered core regions within brain networks, and help mediate global integration of information within and across diverse brain systems[49–51].

They emerge from a very early stage of development and undergo ongoing functional refinement into adulthood[31,33,52,53] as a shift from local to global integrative processing unfolds during adolescence[49]. Functional hubs have been shown to be highly reproducible and consistent in young adults[51]. Relative to non-hubs, functional hubs are involved in a distinctive transcriptomic pattern of neurodevelopmental processes, supporting the development of diverse neuronal connections[51]. Due to their dense connections and topologically central positions, hubs are 'vulnerability hotspots' to dysfunction[32,49,54,55]. The critical and prolonged window of transmodal region maturation is known to be linked to heightened sensitivity to environmental influences[41,56–58]. Deviation from typical hub development during adolescence thus may have a long-lasting impact. This may manifest as pathological organization of brain circuits and abnormal brain functions[49,55,59,60], potentially contributing to the distributed altered functional connectivity observed here.

Taken together, adolescence, coinciding with a protracted period of dramatic plastic changes and significant psychosocial transitions, represents a unique window of increased vulnerability to functional hub system disintegration and in turn altered network dynamics. This likely confers risk for discoordination of a myriad of bottom-up and top-down cognitive, sensory and emotional processes and early emergence of emotional disturbance[61,62], including youth MDD.

The central role of DMN in symptom manifestation

Among all hub regions, the highest consistency was observed for those of the DMN across all analyses. Longitudinal and cross-sectional studies indicate that connectivity within the DMN and its hubs typically strengthens from childhood through adolescence and adulthood. Strengthened connectivity of hubs is thought to underpin optimization of functional integration during brain development[31,32,63]. Interestingly, local hubs of the DMN (for example, mPFC) have been shown to selectively demonstrate strong structure–function coupling during youth (a high correspondence between white matter and functional connectivity), in contrast to the reduced coupling typically observed for all other transmodal regions[64]. This may reflect the unique role of the DMN in supporting coordinated communication between networks among strongly interconnected hub areas within the DMN[65–67].

Notably, our findings indicate multiple associations between DMN connectivity and youth depression severity, implicating DMN dysconnectivity as a central factor. Higher depression severity was associated with stronger anticorrelation in functional connectivity between the DMN and other networks, specifically with DAN, VAN and CEN, in addition to DMN intra-network hyperconnectivity. DMN abnormalities have been widely implicated in altered introspection and excessive rumination in youth and adult MDD[68–72]. The role of DMN anticorrelation with attentional and executive networks is of particular interest. One interpretation of anticorrelated connectivity is an inhibitory relation between networks[73]. The 'one-to-many' networks relation observed here aligns well with past findings of an inhibitory influence of the DMN on attentional and executive networks that have been linked with excessive internal focus[74], cognitive vulnerability[75], and response to treatment in MDD[72]. Taken together, our observed DMN abnormalities may therefore reflect interference with normal communication across introspective and attentional systems. Specifically, top-down attentional and executive control in the competitive selection of bottom-up sensory information and internal mental representation may be particularly compromised in youth MDD secondary to DMN dominance[71,72,76]. This overweighting of DMN input may in turn contribute to maladaptive rumination and negatively biased self-representations and appraisals[68–71,77]. This would be supported by the broader association of DMN abnormalities with internalizing psychopathology dimension in a large cohort of preadolescents, both with and without lifetime mental disorder diagnosis[78].

Critically, in unaffected children with a familial risk of MDD, reduced functional connectivity between regions of the DMN and CEN and heightened DMN connectivity has been reported[79], with DMN–CEN alterations associated with later development of MDD at follow-up[80]. In adult cohorts, drawing from evidence in studies examining antidepressant treatment mechanisms, functional connectivity abnormalities of the DMN are among the most consistently implicated in clinical improvement across pharmacological, invasive and noninvasive brain stimulation treatment (see systematic reviews in refs. 70,81–84 and meta-analysis in ref. 85). Together, DMN aberrancy in at-risk children preceding disease onset and robust normalization of DMN connectivity following antidepressant and noninvasive brain stimulation treatment lend strong support to the role of the DMN as centrally involved in MDD (see reviews in refs. 82,83,86,87).

Implications for neuromodulatory therapeutics

Finally, the most salient features from our machine-learning analysis are in keeping with those implicated in our empirical between-group and symptom severity correlational analyses. Perhaps these features could contribute to neurobiologically informed therapeutic brain stimulation targets in youth MDD. For example, transcranial magnetic stimulation (TMS) has the potential to capitalize on the relatively higher degree of plasticity of the adolescent brain[59]. To date, TMS targets developed for adult depression have been implemented in youth MDD as a best-guess approach to treatment. This includes scalp-based targeting heuristics derived from adult MDD that appear inappropriate for smaller scalp dimensions in youth. Interestingly, recent work has suggested that TMS targeted to sites of the dorsolateral PFC with connectivity to the SGC may be particularly relevant or effective in adult depression[14,88–95]. The strong SGC involvement observed in the present work across analyses indicates that testing TMS targeted to sites connected to the SGC may also be warranted in younger patients. Our work also implicates a range of hub regions that could serve as alternative disease-modifying neuromodulatory therapeutic targets, in line with a recent modeling study implicating largely the same set of regions promoting transitions of brain states between MDD and health elicited by excitatory or inhibitory perturbations[96]. Given the increasingly recognized network-based TMS-induced neuromodulation[97–100], the centrality of these hub regions may be harnessed and potentially serve as 'treatment hotspots' capable of normalizing distributed inter-network abnormalities underpinning youth MDD.

Strengths, limitations and future directions

This work aimed to elucidate robust functional architecture of youth MDD on both individual and group levels and across the scales of functional connections and canonical networks. Compilation of multiple independent cohort datasets in the present study offers the advantages of substantially increased statistical power and more accurate and stable predictive modeling[101], especially when considering the small sample sizes used in past MDD machine-learning studies (see reviews in refs. 26,27).

Several factors, however, may have impacted the statistical power and accuracy of the symptom severity predictive model. First, to maximize the clinical sample, we used established conversion scales for the MADRS[29,30]. These scales require assumptions and may have limited our findings by introducing potential discrepancies in the estimation of symptom severity. More important, the inclusion of both randomized controlled trial and community cohorts further increased clinical heterogeneity[102], evidenced by significant site differences in MADRS. While sample heterogeneity is helpful for identifying reliable neurobiological features that are generalizable and robust in youth MDD, an assumption of harmonization methods such as ComBat is that covariates of interest do not significantly vary across sites[103]. Given that this assumption was not met, we regressed site effects for all our symptom severity-related analyses. Further expansion of the sample size in future work may be one potential solution to help reduce susceptibility to the impact of site-related variance.

Relatedly, the current study can be expanded, and its results may be followed up in several ways. For example, the present approach does not consider dynamic psychosocial or environmental influences on neurodevelopment, and inclusion of such measures could add value to more-comprehensive predictive models in future work. As previously discussed, future effort into examining treatment-related functional connectivity changes is required to better understand mechanisms of action. Leveraging dimension reduction techniques, differential response to treatment associated with distinct clusters of clinical and/or demographic characteristics (phenotypic subtypes) could be identified, as demonstrated in adult MDD[12,104,105]. In youth MDD, different symptom clusters have been found to display differential response to antidepressant treatment[106]. However, the underlying functional connectivity characteristics have remained unexplored. Such investigation would also help shed light on the clinical utility of functional connectivity features as prognostic indicators in guiding treatment selection. In relation, our ethnically and racially diverse cohort presented opportunities for analysis of potential divergence in functional connectivity profiles. However, the need to remove scanner-dependent effects via harmonization is likely to have substantially removed variances associated with ethnicity as certain sites encompassed a predominantly white (Sites 1 and 4) or Asian (Site 5) sample. Separate analysis of large datasets involving specific ethnic groups, such as the REST-meta-MDD Consortium established in China, may help delineate ethnic differences in MDD-related functional connectivity signatures. While our findings can be interpreted in the framework of neurodevelopmental susceptibility and MDD vulnerability, another possibility is that these functional connectivity changes may emerge following symptom onset via activity-dependent processes, and perhaps the default mode and attentional subsystems are most sensitive in this regard. Further longitudinal work is needed to delineate the complex interplay between symptom and functional connectivity alteration manifestations. For example, examination of the interaction between brain maturation and age and divergence of connectivity patterns in MDD versus the healthy comparisons group could be considered. Last, the current work represents an important first step toward establishing robust functional architecture in youth MDD; replication of current findings through future well-powered whole-brain analyses akin to those conducted here would be imperative.

Conclusion

To our knowledge, this work represents the largest pooled multisite resting-state fMRI analysis of brain connectivity and network alterations in youth MDD to date. Our data-driven, connectome-wide functional connectivity and machine-learning analyses converge to consistently implicate involvement of the DMN, DAN and VAN. These connectivity features additionally were able to significantly predict MDD diagnostic status and symptom severity. Crucially, this extensive network involvement in youth MDD localized to regions known to be network hubs. Adolescence, coinciding with a critical period of global network configuration and significant psychosocial transitions, may translate to increased susceptibility to altered hub maturation. This in turn may augment risk for discoordination of internal and external attentional and introspective representations, and ultimately vulnerability to major depression. Importantly, the topological properties of these hub regions may represent opportunities for noninvasive neuromodulatory intervention refinement of potential stimulation targets, capitalizing on the high degree of neural plasticity of the adolescent brain.

Methods

Participants

Structural and resting-state fMRI data were collated across 7 existing cohorts from previously published studies, scanned at 6 international sites, yielding a combined sample of 1,075 young participants (aged 12–25 years)[107–116]. The corresponding authors for each cohort are C.G.D., I.H.G., B.J.H., T.C.H., J.Q., J.S. and T.T.Y., respectively. Cohorts for inclusion in the planned mega-analysis were identified from database searches for journal articles that investigated resting-state functional connectivity in youth MDD (irrespective of the inclusion of a healthy comparison group), published until February 2022. Corresponding authors of appropriate studies were contacted between May 2022 and August 2022 and invited to contribute data to the mega-analysis. The combined sample comprised 488 young individuals with a confirmed diagnosis of MDD and 587 healthy comparison individuals. Brain imaging was performed across six sites in Australia, China, the United Kingdom and the United States. Following quality control, the final sample included 440 youths with MDD and 370 healthy comparison

individuals aged between 12 and 25 years (528 female and 282 male participants; Table 1).

Diagnostic assessments varied across cohorts and consisted of either the K-SADS-PL or the SCID based on the *Diagnostic and Statistical Manual of Mental Disorders* 4th Edition[117] diagnostic criteria (Table 2).

Assessment of depression symptom severity and score conversion

The CDRS-R[29] and HAMD-17[30] scores were transformed into MADRS scores using conversion scales provided in the psychometric validation studies for each respective scale. The conversion of CDRS-R scores produced a score bin (for example, 1–3, 4–5; Supplementary Table 3) while a continuous score was derived from the HAMD-17 conversion. To ensure comparability between individuals, the converted MADRS score bins and continuous scores as well as the original raw scores were then ranked (Supplementary Table 3), yielding a MADRS band score for each MDD individual. This maintains consistency in the assessment of depressive symptom severity across different rating scales, utilizing MADRS band scores as a common metric. MADRS band scores were available for six of the seven clinical cohorts from five scanning sites (with the exception of Site 4). These band scores were used in all subsequent symptom severity analyses.

Ethics approval

A waiver of consent for this study was obtained and approved by the University of Melbourne Human Research Ethics Committees (2022-24565-31548-4). In addition, each site obtained ethics approval from their respective ethics committee for the sharing of anonymized data.

Neuroimaging data

Contributing sites provided structural MRI of brain anatomy (T1 images) and unprocessed resting-state fMRI images for all participants. Unprocessed images were required to enable standardized data pre-processing for all sites. Structural images were used to facilitate registration and normalization of images to the FMRIB Software Library (FSL)'s Montreal Neurological Institute (MNI) ICBM 152 nonlinear 6th Generation Asymmetric Average Brain Stereotaxic Registration Model (MNI152NLin6Asym)[118]. Resting-state fMRI images were used to map functional brain networks (connectomes). MRI acquisition parameters varied between sites (Supplementary Table 4). Mapped connectomes were harmonized to account for site differences (see the following).

Standardized pre-processing and quality control of resting-state fMRI data

Pre-processing was performed using fMRIPrep version 23.0.1[119] which was based on Nipype 1.8.5[120] Pre-processing procedures are detailed in the Supplementary Section 4. Output reports of all pre-processed scans were individually inspected, and exclusion of scans secondary to artifacts (for example, braces), pathologies/incidental findings, unsuccessful pre-processing and/or poor quality of pre-processed scans (for example, poor anatomical and functional registration, poor field of view) was established by consensus among investigators, N.Y.T., R.F.H.C. and A.Z. To ensure that current findings were unlikely to be biased by potential confounding influences of head motion, individuals with a mean framewise displacement (FD) > 2 mm or standardized DVARS (the derivative of root mean square variance over voxels[121]) > 1.5 and/or FD > 0.5 mm for more than 20% of the volumes (outlier volumes) were excluded. Participant exclusion rates at each stage of analysis are detailed in Extended Data Fig. 1. The mean FD, standardized DVARS and RMSD[122] values and percentage of outlier volumes were also included as an additional covariate in supplementary NBS analyses (Supplementary Section 3) and compared between the final MDD and control groups to account for a potential disproportionate influence of head motion. For further head motion artifact removal, additional supplementary analyses, adopting a more stringent exclusion criteria of mean FD > 1.5 mm and 20% outlier volumes, were conducted.

The first four volumes were discarded to ensure steady state. The 24 head motion parameters and their derivatives[123], as well as signals from white matter, cerebrospinal fluid and global signal, were regressed from the processed fMRI time series, and the resulting residuals were used for connectome mapping. Regressors from discrete cosine transformation basis functions were also included for high-pass filtering. Global signal regression was used to further alleviate head motion[124,125], given that the population studied may be susceptible to motion artifacts[54]. Supplementary analyses without the application of global signal regression were also conducted (Supplementary Section 3).

Functional connectome mapping. The Schaefer–Yeo 7-network functional atlas[126] was used to parcellate the cortex into 400 volumetric functional parcels, and the Melbourne Subcortical Atlas[127] was used to parcellate the subcortex into 54 functional nuclei, yielding a total of 454 regions. The 400 cortical parcellation was chosen per previous recommendations[128]. Each cortical region was assigned to one of seven canonical resting-state functional networks[126,129]: DMN, VAN, SMN, limbic network, visual network, DAN and CEN (also known as frontoparietal). For each participant, the pre-processed resting-state fMRI time series was spatially averaged across all voxels composing each region, yielding an averaged time series for each region. The Pearson correlation coefficient was computed between all pairs of regions from the combined cortical and subcortical atlases to provide a measure of functional connectivity, yielding a 454 × 454 symmetric connectivity matrix for each individual. ComBat[130] leverages multivariate linear mixed-effects regression and empirical Bayes to correct batch effects (systematic differences among data collected from diverse batches/sites). We applied this methodology to harmonize functional connectivity matrices while retaining variance of interest (age, sex and diagnosis). ComBat was chosen due to previous mega-analytical studies demonstrating its effectiveness in substantially removing site-specific artifacts in multi-site resting-state fMRI across diverse functional connectivity metrics[131–133].

Statistical inference

The NBS[28] was used to test for between-group differences in functional connectivity. The NBS ensures control of the family-wise error rate across the set of all functional connections tested. As such, it is widely used in psychopathology research, including whole brain-based mega-analytical work[132], capitalizing on its ability to address multiple comparison issues inherent in connectome-wide analysis. Specifically, using the functional matrices, the NBS statistically localized subnetworks of connections with increased or decreased connectivity in the MDD group compared with the healthy comparison individuals. All NBS between-group analyses were adjusted for age and sex. The NBS was also used to identify connections for which variation in connectivity strength across MDD individuals was associated with variation in symptom severity, as measured using the MADRS. Harmonization was repeated for this subset of individuals to preserve variance explained by age and sex, as well as MADRS score. Considering the significant differences in MADRS between sites (Table 2) and the tacit assumption of ComBat that covariates of interest are not strongly correlated with sites (see ref. 103) for a detailed discussion), we directly controlled for site effect by regressing out the effect of site from MADRS scores before ComBat harmonization. The NBS was used to separately test for positive and negative associations between functional connectivity and MADRS. Regions harboring the highest total number of significant connections were considered salient regions.

An edge-forming threshold of $t > 3.5$ was used. Family-wise error correction at $P < 0.05$ was deemed statistically significant, and 5,000 permutations were generated to estimate the null distribution for the NBS. To ensure absence of site influence on MADRS in harmonization

and subsequent brain–behavior associations, the resultant correlational NBS findings were compared with chance level using permutation testing. This involved randomly permuting site-regressed MADRS scores among individuals within each site to generate a null dataset where any potential association between functional connectivity and MADRS is eliminated. Multiple instantiations of such null datasets were generated ($N = 1{,}500$), and the exact same ComBat harmonization and NBS correlational analysis pipeline was repeated for each null dataset. This revealed that approximately 5% of the 1,500 null distribution samples yielded a significant subnetwork linked with depression symptom severity for positive and negative association ($P < 0.05$), respectively, confirming satisfactory control of false positive rates.

Supplementary NBS analyses were also performed to explore whether unique patterns of functional connectivity changes may be associated with distinct demographic and/or clinical profiles. First, we repeated the between-group NBS analyses with the additional inclusion of age-by-diagnosis and sex-by-diagnosis interaction terms to delineate potential age and sex interaction effects. An additional between-group comparison was also conducted to assess the effect of medication history by comparing functional connectivity between patients with ($n = 68$) and without ($n = 190$) a history of antidepressant intervention, with age and sex included as covariates. The same statistical threshold was applied for all supplementary NBS analyses.

The assumption of normality and equal variances was not formally tested as the statistical tests used to derive functional connectivity markers of youth MDD do not make any assumptions regarding data distribution.

Predictive modeling of diagnostic status and depression severity

Support vector machines (SVMs) were trained to predict individual diagnostic status and MADRS score on the basis of functional connectivity profiles. ComBat was first implemented to harmonize functional connectivity matrices with relevant variables of interest retained for the classification (diagnosis, age and sex; $n = 810$) and regression (MADRS, age and sex; $n = 348$ youths with MDD) samples, respectively. To mitigate the potential impact of significant site differences in MADRS on harmonization and regression modeling, we regressed the effect of site from MADRS before ComBat harmonization. Following harmonization, data were first partitioned into training and test sets using leave-one-site-out cross-validation (Fig. 1). Partitioning was performed such that N − 1 sites were used for model training while the remaining site was reserved as the test set. Functional connectivity data were summarized in the form of a matrix X of dimensions $M \times 102{,}831$ matrix, where M is the number of individuals composing the training set and 102,831 is the number of unique functional connections ($454 \times 453/2 = 102{,}831$ upper diagonal elements). Note that M changed for each cross-validation fold. To reduce the dimensionality of the functional connectivity space, PCA was applied to X, yielding a $102{,}831 \times M - 1$ matrix of principal component coefficients, C, and a corresponding $M \times M - 1$ matrix of principal component scores, S. The PCA decomposition could be represented as $X = SC'$. The SVM was trained using the top 60 principal component scores stored in S.

The SVM classification and regression were implemented using the fitclinear and fitrlinear functions, respectively, in MATLAB. Models were fitted with stochastic gradient descent, and ridge regularization was performed with the default regularization term strength of $\lambda = 1/M$. Model performance could potentially be improved by optimizing this hyperparameter, but this was not considered in the current study. Accuracy was evaluated on the test set as follows. Let X_{test} denote the equivalent of X for the test set. We first projected X_{test} into the space of the principal components, such that $\bar{X}_{\text{test}} = X_{\text{test}}C$, and then applied the fitted model to $\bar{X}_{test}$ to derive predictions for individuals composing the test set. Given the stochastic nature of the model-fitting algorithm (stochastic gradient descent), the entire model-fitting and evaluation process was repeated 100 times, and model performance was averaged across the 100 iterations, unless otherwise stated.

To assist with interpretability of the feature weights, they were transformed using the Haufe transformation[34,134]. The relative contribution of each of the seven networks to prediction performance was also examined (see Supplementary Section 5 for details).

To explore the sole contribution of demographic variables to classification performance, we trained an SVM classifier to classify diagnostic status on the basis of age and sex, as well as age alone. This established a benchmark/reference prediction accuracy.

Last, permutation testing was used to estimate a P value to exclude any parametric assumptions. This involved permuting site-regressed MADRS scores among individuals within each site before the application of ComBat and SVM regression analyses. This procedure was repeated 1,500 times to generate an empirical null distribution. We found that the observed r value was greater than that obtained from permutations in 1,483 of 1,500 trials ($P = 0.011$), confirming that the observed strength of correlation was significantly stronger than would be expected by chance.

Reporting summary

Further information on research design is available in the Nature Portfolio Reporting Summary linked to this article.

Data availability

This study did not involve the use of publicly available datasets, but de-identified data from seven previously published datasets collected by six research groups across four countries. Data may be made available upon reasonable request at the discretion of each respective principal investigator. Data sharing will be subject to the policies and procedures of the institution where each dataset was collected. Principal investigators from sites that provided data used in this study include C.G.D. (Sites 1 and 2), I.H.G. (Site 3 TAD dataset), B.J.H. (Sites 1 and 2), T.C.H. (Site 3 TIGER dataset), J.Q. (Site 5), J.S. (Site 4) and T.T.Y. (Site 6). Please direct all data requests to N.Y.T. at ngayant@student.unimelb.edu.au.

Code availability

All the neuroimaging pre-processing and analyses conducted in this study involved the use of publicly available toolboxes and resources. This included the fMRIPrep version 23.0.1 (accessible at https://fmriprep.org/en/stable/installation.html), the combined Schaefer 400 cortical and Melbourne Subcortex Atlas (accessible at https://github.com/yetianmed/subcortex/tree/master/Group-Parcellation/3T/Cortex-Subcortex), NBS MATLAB toolbox version 1.2 (accessible at https://www.nitrc.org/projects/nbs/) and ComBat Harmonization package (https://github.com/Jfortin1/ComBatHarmonization). All cortical renderings were generated using the GUI-based toolbox BrainNet Viewer version 1.7 (https://www.nitrc.org/projects/bnv) via MATLAB. For predictive analyses, dimension reduction via PCA was performed using the pca function in MATLAB version R2021a. This was followed by classification and regression analyses performed using the fitclinear and fitrlinear MATLAB functions, respectively.

References

1. Kessler, R. C. & Bromet, E. J. The epidemiology of depression across cultures. *Annu. Rev. Public Health* **34**, 119–138 (2013).
2. Kovess-Masfety, V. et al. Irritable mood in adult major depressive disorder: results from the world mental health surveys. *Depress. Anxiety* **30**, 395–406 (2013).
3. Gore, F. M. et al. Global burden of disease in young people aged 10–24 years: a systematic analysis. *Lancet* **377**, 2093–2102 (2011).
4. Vos, T. et al. Global, regional, and national incidence, prevalence, and years lived with disability for 310 diseases and injuries, 1990–2015: a systematic analysis for the Global Burden of Disease Study 2015. *Lancet* **388**, 1545–1602 (2016).

5. Dold, M. & Kasper, S. Evidence-based pharmacotherapy of treatment-resistant unipolar depression. *Int. J. Psychiatry Clin. Pract.* **21**, 13–23 (2017).
6. Zisook, S. et al. Preadult onset vs. adult onset of major depressive disorder: a replication study. *Acta Psychiatr. Scand.* **115**, 196–205 (2007).
7. Kessler, R. C. The costs of depression. *Psychiatr. Clin. North Am.* **35**, 1–14 (2012).
8. Iorfino, F., Hickie, I. B., Lee, R. S. C., Lagopoulos, J. & Hermens, D. F. The underlying neurobiology of key functional domains in young people with mood and anxiety disorders: a systematic review. *BMC Psychiatry* **16**, 156 (2016).
9. Johnson, D., Dupuis, G., Piche, J., Clayborne, Z. & Colman, I. Adult mental health outcomes of adolescent depression: a systematic review. *Depress. Anxiety* **35**, 700–716 (2018).
10. Menon, V. Large-scale brain networks and psychopathology: a unifying triple network model. *Trends Cogn. Sci.* **15**, 483–506 (2011).
11. Bressler, S. L. & Menon, V. Large-scale brain networks in cognition: emerging methods and principles. *Trends Cogn. Sci.* **14**, 277–290 (2010).
12. Siddiqi, S. H. et al. Distinct symptom-specific treatment targets for circuit-based neuromodulation. *Am. J. Psychiatry* **177**, 435–446 (2020).
13. Cash, R. F. H. et al. Using brain imaging to improve spatial targeting of transcranial magnetic stimulation for depression. *Biol. Psychiatry* https://doi.org/10.1016/j.biopsych.2020.05.033 (2020).
14. Siddiqi, S. H. et al. Brain stimulation and brain lesions converge on common causal circuits in neuropsychiatric disease. *Nat. Hum. Behav.* **5**, 1707–1716 (2021).
15. Cash, R. F. H., Müller, V. I., Fitzgerald, P. B., Eickhoff, S. B. & Zalesky, A. Altered brain activity in unipolar depression unveiled using connectomics. *Nat. Ment. Health* **1**, 174–185 (2023).
16. Van Essen, D. C. & Barch, D. M. The human connectome in health and psychopathology. *World Psychiatry* **14**, 154–157 (2015).
17. Ashworth, E., Brooks, S. J. & Schiöth, H. B. Neural activation of anxiety and depression in children and young people: a systematic meta-analysis of fMRI studies. *Psychiatry Res. Neuroimaging* **311**, 111272 (2021).
18. Tse, N. Y., Ratheesh, A., Ganesan, S., Zalesky, A. & Cash, R. F. H. Functional dysconnectivity in youth depression: systematic review, meta-analysis, and network-based integration. *Neurosci. Biobehav. Rev.* **153**, 105394 (2023).
19. Botvinik-Nezer, R. et al. Variability in the analysis of a single neuroimaging dataset by many teams. *Nature* **582**, 84–88 (2020).
20. Marek, S. et al. Reproducible brain-wide association studies require thousands of individuals. *Nature* **603**, 654–660 (2022).
21. Poldrack, R. A. et al. Scanning the horizon: towards transparent and reproducible neuroimaging research. *Nat. Rev. Neurosci.* **18**, 115–126 (2017).
22. Onitsuka, T. et al. Trends in big data analyses by multicenter collaborative translational research in psychiatry. *Psychiatry Clin. Neurosci.* **76**, 1–14 (2022).
23. Thompson, P. M. et al. ENIGMA and global neuroscience: a decade of large-scale studies of the brain in health and disease across more than 40 countries. *Transl. Psychiatry* **10**, 100 (2020).
24. Zacharek, S. J., Kribakaran, S., Kitt, E. R. & Gee, D. G. Leveraging big data to map neurodevelopmental trajectories in pediatric anxiety. *Dev. Cogn. Neurosci.* **50**, 100974 (2021).
25. Zugman, A. et al. Mega-analysis methods in ENIGMA: the experience of the generalized anxiety disorder working group. *Hum. Brain Mapp.* **43**, 255–277 (2022).
26. Gao, S., Calhoun, V. D. & Sui, J. Machine learning in major depression: from classification to treatment outcome prediction. *CNS Neurosci. Ther.* **24**, 1037–1052 (2018).
27. Patel, M. J., Khalaf, A. & Aizenstein, H. J. Studying depression using imaging and machine learning methods. *Neuroimage Clin.* **10**, 115–123 (2016).
28. Zalesky, A., Fornito, A. & Bullmore, E. T. Network-based statistic: identifying differences in brain networks. *Neuroimage* **53**, 1197–1207 (2010).
29. Jain, S. et al. A psychometric evaluation of the CDRS and MADRS in assessing depressive symptoms in children. *J. Am. Acad. Child Adolesc. Psychiatry* **46**, 1204–1212 (2007).
30. Leucht, S., Fennema, H., Engel, R. R., Kaspers-Janssen, M. & Szegedi, A. Translating the HAM-D into the MADRS and vice versa with equipercentile linking. *J. Affect. Disord.* **226**, 326–331 (2018).
31. Oldham, S. & Fornito, A. The development of brain network hubs. *Dev. Cogn. Neurosci.* **36**, 100607 (2019).
32. van den Heuvel, M. P. & Sporns, O. Network hubs in the human brain. *Trends Cogn. Sci.* **17**, 683–696 (2013).
33. Kaiser, M. Mechanisms of connectome development. *Trends Cogn. Sci.* **21**, 703–717 (2017).
34. Haufe, S. et al. On the interpretation of weight vectors of linear models in multivariate neuroimaging. *Neuroimage* **87**, 96–110 (2014).
35. Sacchet, M. D. et al. Large-scale hypoconnectivity between resting-state functional networks in unmedicated adolescent major depressive disorder. *Neuropsychopharmacology* **41**, 2951–2960 (2016).
36. Gray, J. P., Müller, V. I., Eickhoff, S. B. & Fox, P. T. Multimodal abnormalities of brain structure and function in major depressive disorder: a meta-analysis of neuroimaging studies. *Am. J. Psychiatry* **177**, 422–434 (2020).
37. Kaiser, R. H., Andrews-Hanna, J. R., Wager, T. D. & Pizzagalli, D. A. Large-scale network dysfunction in major depressive disorder: a meta-analysis of resting-state functional connectivity. *JAMA Psychiatry* **72**, 603–611 (2015).
38. Dai, L., Zhou, H., Xu, X. & Zuo, Z. Brain structural and functional changes in patients with major depressive disorder: a literature review. *PeerJ* https://doi.org/10.7717/peerj.8170 (2019).
39. Li, X. & Wang, J. Abnormal neural activities in adults and youths with major depressive disorder during emotional processing: a meta-analysis. *Brain Imaging Behav.* **15**, 1134–1154 (2021).
40. Zhukovsky, P. et al. Coordinate-based network mapping of brain structure in major depressive disorder in younger and older adults: a systematic review and meta-analysis. *Am. J. Psychiatry* **178**, 1119–1128 (2021).
41. Kolk, S. M. & Rakic, P. Development of prefrontal cortex. *Neuropsychopharmacology* **47**, 41–57 (2022).
42. Gogtay, N. et al. Dynamic mapping of human cortical development during childhood through early adulthood. *Proc. Natl Acad. Sci.* **101**, 8174–8179 (2004).
43. Casanova, R., Whitlow, C. T., Wagner, B., Espeland, M. A. & Maldjian, J. A. Combining graph and machine learning methods to analyze differences in functional connectivity across sex. *Open Neuroimag. J.* https://doi.org/10.2174/1874440001206010001 (2012).
44. Zhang, C., Dougherty, C. C., Baum, S. A., White, T. & Michael, A. M. Functional connectivity predicts gender: evidence for gender differences in resting brain connectivity. *Hum. Brain Mapp.* **39**, 1765–1776 (2018).
45. Korgaonkar, M. S., Goldstein-Piekarski, A. N., Fornito, A. & Williams, L. M. Intrinsic connectomes are a predictive biomarker of remission in major depressive disorder. *Mol. Psychiatry* **25**, 1537–1549 (2020).
46. Chin Fatt, C. R. et al. Effect of intrinsic patterns of functional brain connectivity in moderating antidepressant. *Am. J. Psychiatry* **177**, 143–154 (2020).

47. Liston, C. et al. Default mode network mechanisms of transcranial magnetic stimulation in depression. *Biol. Psychiatry* **76**, 517–526 (2014).
48. Toenders, Y. J. et al. Neuroimaging predictors of onset and course of depression in childhood and adolescence: a systematic review of longitudinal studies. *Dev. Cogn. Neurosci.* **39**, 100700 (2019).
49. van den Heuvel, M. P. & Sporns, O. A cross-disorder connectome landscape of brain dysconnectivity. *Nat. Rev. Neurosci.* **20**, 435–446 (2019).
50. Bullmore, E. & Sporns, O. Complex brain networks: graph theoretical analysis of structural and functional systems. *Nat. Rev. Neurosci.* **10**, 186–198 (2009).
51. Xu, Z. et al. Meta-connectomic analysis maps consistent, reproducible, and transcriptionally relevant functional connectome hubs in the human brain. *Commun. Biol.* **5**, 1056 (2022).
52. Grayson, D. S. et al. Structural and functional rich club organization of the brain in children and adults. *PLoS ONE* **9**, e88297 (2014).
53. Grayson, D. S. & Fair, D. A. Development of large-scale functional networks from birth to adulthood: a guide to the neuroimaging literature. *Neuroimage* **160**, 15–31 (2017).
54. van den Heuvel, M. P., Scholtens, L. H. & Kahn, R. S. Multiscale neuroscience of psychiatric disorders. *Biol. Psychiatry* **86**, 512–522 (2019).
55. Fornito, A., Bullmore, E. T. & Zalesky, A. Opportunities and challenges for psychiatry in the connectomic era. *Biol. Psychiatry Cogn. Neurosci. Neuroimaging* **2**, 9–19 (2017).
56. Sisk, L. M. & Gee, D. G. Stress and adolescence: vulnerability and opportunity during a sensitive window of development. *Curr. Opin. Psychol.* **44**, 286–292 (2022).
57. Sydnor, V. J. et al. Intrinsic activity development unfolds along a sensorimotor–association cortical axis in youth. *Nat. Neurosci.* https://doi.org/10.1038/s41593-023-01282-y (2023).
58. Sydnor, V. J. et al. Neurodevelopment of the association cortices: patterns, mechanisms, and implications for psychopathology. *Neuron* **109**, 2820–2846 (2021).
59. Marín, O. Developmental timing and critical windows for the treatment of psychiatric disorders. *Nat. Med.* **22**, 1229–1238 (2016).
60. Ho, T. C. & King, L. S. Mechanisms of neuroplasticity linking early adversity to depression: developmental considerations. *Transl. Psychiatry* **11**, 517 (2021).
61. Giedd, J. N., Keshavan, M. & Paus, T. Why do many psychiatric disorders emerge during adolescence. *Nat. Rev. Neurosci.* **9**, 947–957 (2008).
62. Casey, B. J., Heller, A. S., Gee, D. G. & Cohen, A. O. Development of the emotional brain. *Neurosci. Lett.* **693**, 29–34 (2019).
63. Sotiras, A. et al. Patterns of coordinated cortical remodeling during adolescence and their associations with functional specialization and evolutionary expansion. *Proc. Natl Acad. Sci. USA* **114**, 3527–3532 (2017).
64. Baum, G. L. et al. Development of structure–function coupling in human brain networks during youth. *Proc. Natl Acad. Sci. USA* **117**, 771–778 (2020).
65. Buckner, R. L. & DiNicola, L. M. The brain's default network: updated anatomy, physiology and evolving insights. *Nat. Rev. Neurosci.* **20**, 593–608 (2019).
66. Andrews-Hanna, J. R. The brain's default network and its adaptive role in internal mentation. *Neuroscientist* **18**, 251–270 (2012).
67. Andrews-Hanna, J. R., Reidler, J. S., Sepulcre, J., Poulin, R. & Buckner, R. L. Functional-anatomic fractionation of the brain's default network. *Neuron* **65**, 550–562 (2010).
68. Hamilton, J. P., Farmer, M., Fogelman, P. & Gotlib, I. H. Depressive rumination, the default-mode network, and the dark matter of clinical neuroscience. *Biol. Psychiatry* **78**, 224–230 (2015).
69. Zhou, H. X. et al. Rumination and the default mode network: meta-analysis of brain imaging studies and implications for depression. *Neuroimage* **206**, 116287 (2020).
70. Li, B. J. et al. A brain network model for depression: from symptom understanding to disease intervention. *CNS Neurosci. Ther.* **24**, 1004–1019 (2018).
71. Davey, C. G. & Harrison, B. J. The self on its axis: a framework for understanding depression. *Transl. Psychiatry* **12**, 23 (2022).
72. Jamieson, A. J., Harrison, B. J., Razi, A. & Davey, C. G. Rostral anterior cingulate network effective connectivity in depressed adolescents and associations with treatment response in a randomized controlled trial. *Neuropsychopharmacology* **47**, 1240–1248 (2022).
73. Uddin, L. Q., Kelly, A. M. C., Biswal, B. B., Castellanos, F. X. & Milham, M. P. Functional connectivity of default mode network components: correlation, anticorrelation, and causality. *Hum. Brain Mapp.* **30**, 625–637 (2009).
74. Hamilton, J. P. et al. Default-mode and task-positive network activity in major depressive disorder: implications for adaptive and maladaptive rumination. *Biol. Psychiatry* **70**, 327–333 (2011).
75. Wang, X., Öngür, D., Auerbach, R. P. & Yao, S. Cognitive vulnerability to major depression: view from the intrinsic network and cross-network interactions. *Harv. Rev. Psychiatry* **24**, 188–201 (2016).
76. Andrews-Hanna, J. R., Smallwood, J. & Spreng, R. N. The default network and self-generated thought: component processes, dynamic control, and clinical relevance. *Ann. N. Y. Acad. Sci.* **1316**, 29–52 (2014).
77. Davey, C. G., Breakspear, M., Pujol, J. & Harrison, B. J. A brain model of disturbed self-appraisal in depression. *Am. J. Psychiatry* **174**, 895–903 (2017).
78. Lees, B. et al. Altered neurocognitive functional connectivity and activation patterns underlie psychopathology in preadolescence. *Biol. Psychiatry Cogn. Neurosci. Neuroimaging* **6**, 387–398 (2021).
79. Chai, X. J. et al. Altered intrinsic functional brain architecture in children at familial risk of major depression. *Biol. Psychiatry* **80**, 849–858 (2016).
80. Hirshfeld-Becker, D. R. et al. Intrinsic functional brain connectivity predicts onset of major depression disorder in adolescence: a pilot study. *Brain Connect.* **9**, 388–398 (2019).
81. Dunlop, K., Talishinsky, A. & Liston, C. Intrinsic brain network biomarkers of antidepressant response: a review. *Curr. Psychiatry Rep.* **21**, 87 (2019).
82. Brakowski, J. et al. Resting state brain network function in major depression—depression symptomatology, antidepressant treatment effects, future research. *J. Psychiatr. Res.* **92**, 147–159 (2017).
83. Tura, A. & Goya-Maldonado, R. Brain connectivity in major depressive disorder: a precision component of treatment modalities? *Transl. Psychiatry* **13**, 196 (2023).
84. Li, J., Chen, J., Kong, W., Li, X. & Hu, B. Abnormal core functional connectivity on the pathology of MDD and antidepressant treatment: a systematic review. *J. Affect. Disord.* **296**, 622–634 (2022).
85. Marwood, L., Wise, T., Perkins, A. M. & Cleare, A. J. Meta-analyses of the neural mechanisms and predictors of response to psychotherapy in depression and anxiety. *Neurosci. Biobehav. Rev.* **95**, 61–72 (2018).
86. Macêdo, M. A., Sato, J. R., Bressan, R. A. & Pan, P. M. Adolescent depression and resting-state fMRI brain networks: a scoping review of longitudinal studies. *Braz. J. Psychiatry* **44**, 420–433 (2022).
87. Taïb, S. et al. How does repetitive transcranial magnetic stimulation influence the brain in depressive disorders?: A review of neuroimaging magnetic resonance imaging studies. *J. ECT* **34**, 79–86 (2018).
88. Fox, M. D., Buckner, R. L., White, M. P., Greicius, M. D. & Pascual-Leone, A. Efficacy of transcranial magnetic stimulation targets for depression is related to intrinsic functional connectivity with the subgenual cingulate. *Biol. Psychiatry* https://doi.org/10.1016/j.biopsych.2012.04.028 (2012).

89. Weigand, A. et al. Prospective validation that subgenual connectivity predicts antidepressant efficacy of transcranial magnetic stimulation sites. *Biol. Psychiatry* **84**, 28–37 (2018).
90. Cash, R. F. H. et al. A multivariate neuroimaging biomarker of individual outcome to transcranial magnetic stimulation in depression. *Hum. Brain Mapp.* **40**, 4618–4629 (2019).
91. Cash, R. F. H., Cocchi, L., Lv, J., Fitzgerald, P. B. & Zalesky, A. Functional magnetic resonance imaging-guided personalization of transcranial magnetic stimulation treatment for depression. *JAMA Psychiatry* **78**, 337–339 (2021).
92. Siddiqi, S. H., Weigand, A., Pascual-Leone, A. & Fox, M. D. Identification of personalized transcranial magnetic stimulation targets based on subgenual cingulate connectivity: an independent replication. *Biol. Psychiatry* **90**, e55–e56 (2021).
93. Cole, E. J. et al. Stanford accelerated intelligent neuromodulation therapy for treatment-resistant depression. *Am. J. Psychiatry* **177**, 716–726 (2020).
94. Cole, E. J. et al. Stanford neuromodulation therapy (SNT): a double-blind randomized controlled trial. *Am. J. Psychiatry* **179**, 132–141 (2022).
95. Moreno-Ortega, M. et al. Parcel-guided rTMS for depression. *Transl. Psychiatry* **10**, 283 (2020).
96. Wang, S. et al. Driving brain state transitions in major depressive disorder through external stimulation. *Hum. Brain Mapp.* **43**, 5326–5339 (2022).
97. Beynel, L., Powers, J. P. & Appelbaum, L. G. Effects of repetitive transcranial magnetic stimulation on resting-state connectivity: a systematic review. *Neuroimage* **211**, 116596 (2020).
98. Philip, N. S., Barredo, J., Aiken, E. & Carpenter, L. L. Neuroimaging mechanisms of therapeutic transcranial magnetic stimulation for major depressive disorder. *Biol. Psychiatry Cogn. Neurosci. Neuroimaging* **3**, 211–222 (2018).
99. Eldaief, M. C. et al. Network-specific metabolic and haemodynamic effects elicited by non-invasive brain stimulation. *Nat. Ment. Health* **1**, 346–360 (2023).
100. Sale, M. V., Mattingley, J. B., Zalesky, A. & Cocchi, L. Imaging human brain networks to improve the clinical efficacy of non-invasive brain stimulation. *Neurosci. Biobehav. Rev.* **57**, 187–198 (2015).
101. Cui, Z. & Gong, G. The effect of machine learning regression algorithms and sample size on individualized behavioral prediction with functional connectivity features. *Neuroimage* **178**, 622–637 (2018).
102. Hetrick, S. E., McKenzie, J. E., Cox, G. R., Simmons, M. B. & Merry, S. N. Newer generation antidepressants for depressive disorders in children and adolescents. *Cochrane Database Syst. Rev.* https://doi.org/10.1002/14651858.CD004851.pub3 (2012).
103. Kim, M. E. et al. Empirical assessment of the assumptions of ComBat with diffusion tensor imaging. *J. Med. Imaging* **11**, 024011 (2024).
104. Drysdale, A. T. et al. Resting-state connectivity biomarkers define neurophysiological subtypes of depression. *Nat. Med.* **23**, 28–38 (2017).
105. Hollunder, B. et al. Toward personalized medicine in connectomic deep brain stimulation. *Prog. Neurobiol.* **210**, 102211 (2022).
106. Bondar, J., Caye, A., Chekroud, A. M. & Kieling, C. Symptom clusters in adolescent depression and differential response to treatment: a secondary analysis of the treatment for adolescents with depression study randomised trial. *Lancet Psychiatry* https://doi.org/10.1016/S2215-0366(20)30060-2 (2020).
107. Cheng, W. et al. Increased functional connectivity of the posterior cingulate cortex with the lateral orbitofrontal cortex in depression. *Transl. Psychiatry* **8**, 90 (2018).
108. Berk, M. et al. Youth depression alleviation with anti-inflammatory agents (YoDA-A): a randomised clinical trial of rosuvastatin and aspirin. *BMC Med.* **18**, 16 (2020).
109. Walker, J. C. et al. Study protocol for teen inflammation glutamate emotion research (TIGER). *Front. Hum. Neurosci.* **14**, 585512 (2020).
110. Ho, T. C. et al. Default mode and salience network alterations in suicidal and non-suicidal self-injurious thoughts and behaviors in adolescents with depression. *Transl. Psychiatry* **11**, 38 (2021).
111. Davey, C. G., Cearns, M., Jamieson, A. & Harrison, B. J. Suppressed activity of the rostral anterior cingulate cortex as a biomarker for depression remission. *Psychol. Med.* **53**, 2448–2455 (2023).
112. Connolly, C. G. et al. Resting-state functional connectivity of the amygdala and longitudinal changes in depression severity in adolescent depression. *J. Affect. Disord.* **207**, 86–94 (2017).
113. Schwartz, J. et al. Resting-state functional connectivity and inflexibility of daily emotions in major depression. *J. Affect. Disord.* **249**, 26–34 (2019).
114. Chattopadhyay, S. et al. Cognitive behavioral therapy lowers elevated functional connectivity in depressed adolescents. *EBioMedicine* **17**, 216–222 (2017).
115. Hagan, C. C. et al. Magnetic resonance imaging of a randomized controlled trial investigating predictors of recovery following psychological treatment in adolescents with moderate to severe unipolar depression: study protocol for Magnetic Resonance-Improving Mood with Psychoanalytic and Cognitive Therapies (MR-IMPACT). *BMC Psychiatry* **13**, 247 (2013).
116. Davey, C. G. et al. The addition of fluoxetine to cognitive behavioural therapy for youth depression (YoDA-C): a randomised, double-blind, placebo-controlled, multicentre clinical trial. *Lancet Psychiatry* **6**, 735–744 (2019).
117. American Psychiatric Association. *Diagnostic and Statistical Manual of Mental Disorders* 4th ed. (APA, 1994).
118. Evans, A. C., Janke, A. L., Collins, D. L. & Baillet, S. Brain templates and atlases. *Neuroimage* **62**, 911–922 (2012).
119. Esteban, O. et al. fMRIPrep: a robust preprocessing pipeline for functional MRI. *Nat. Methods* **16**, 111–116 (2019).
120. Gorgolewski, K. et al. Nipype: a flexible, lightweight and extensible neuroimaging data processing framework in Python. *Front. Neuroinform.* **5**, 13 (2011).
121. Power, J. D., Barnes, K. A., Snyder, A. Z., Schlaggar, B. L. & Petersen, S. E. Spurious but systematic correlations in functional connectivity MRI networks arise from subject motion. *Neuroimage* **59**, 2142–2154 (2012).
122. Jenkinson, M., Bannister, P., Brady, M. & Smith, S. Improved optimization for the robust and accurate linear registration and motion correction of brain images. *Neuroimage* **17**, 825–841 (2002).
123. Friston, K. J., Williams, S., Howard, R., Frackowiak, R. S. J. & Turner, R. Movement-related effects in fMRI time-series. *Magn. Reson. Med.* **35**, 346–355 (1996).
124. Power, J. D. et al. Methods to detect, characterize, and remove motion artifact in resting state fMRI. *Neuroimage* **84**, 320–341 (2014).
125. Ciric, R. et al. Benchmarking of participant-level confound regression strategies for the control of motion artifact in studies of functional connectivity. *Neuroimage* **154**, 174–187 (2017).
126. Schaefer, A. et al. Local–global parcellation of the human cerebral cortex from intrinsic functional connectivity MRI. *Cereb. Cortex* **28**, 3095–3114 (2018).
127. Tian, Y., Margulies, D. S., Breakspear, M. & Zalesky, A. Topographic organization of the human subcortex unveiled with functional connectivity gradients. *Nat. Neurosci.* **23**, 1421–1432 (2020).
128. Van Essen, D. C., Glasser, M. F., Dierker, D. L., Harwell, J. & Coalson, T. Parcellations and hemispheric asymmetries of human cerebral cortex analyzed on surface-based atlases. *Cereb. Cortex* **22**, 2241–2262 (2012).
129. Yeo, B. T. T. et al. The organization of the human cerebral cortex estimated by intrinsic functional connectivity. *J. Neurophysiol.* **106**, 1125–1165 (2011).

130. Johnson, W. E., Li, C. & Rabinovic, A. Adjusting batch effects in microarray expression data using empirical Bayes methods. *Biostatistics* **8**, 118–127 (2007).
131. Yu, M. et al. Statistical harmonization corrects site effects in functional connectivity measurements from multi-site fMRI data. *Hum. Brain Mapp.* **39**, 4213–4227 (2018).
132. Ilioska, I. et al. Connectome-wide mega-analysis reveals robust patterns of atypical functional connectivity in autism. *Biol. Psychiatry* https://doi.org/10.1016/j.biopsych.2022.12.018 (2023).
133. Du, X. et al. Unraveling schizophrenia replicable functional connectivity disruption patterns across sites. *Hum. Brain Mapp.* **44**, 156–169 (2023).
134. Tian, Y. & Zalesky, A. Machine learning prediction of cognition from functional connectivity: are feature weights reliable? *Neuroimage* **245**, 118648 (2021).
135. Xia, M., Wang, J. & He, Y. BrainNet Viewer: a network visualization tool for human brain connectomics. *PLoS ONE* **8**, e68910 (2013).

Acknowledgments

This work was supported by the American Foundation for Suicide Prevention (SRG-1-141-18 to T.T.Y.), the Australian National Health and Medical Research Council (NHMRC; Postgraduate Scholarship grant no. 2022387 to N.Y.T., Early Career fellowship to A.R., Investigator Leadership grant no. 2017962 to L.S. and Emerging Leadership Investigator grant no. 2017527 to R.F.H.C.), the Australian Research Council Future Fellowship (A.Z.), the Australian Research Training Program Scholarship (S.G.), the Brain and Behavior Research Foundation (to T.T.Y. and grant no. 28972 to M.D.S.), the Dimension Giving Fund (M.D.S.), the training fellowship awarded to the Division of Child and Adolescent Psychiatry at Columbia University (grant no. T32 MH016434-42 to J.S.K.), the Graeme Clark Institute top-up scholarship (S.G.), the J. Jacobson Fund (T.T.Y.), the Mary Lugton Postdoc Fellowship (Y.E.T.), the National Center for Advancing Translational Sciences (T.T.Y.), the National Center for Complementary and Integrative Health (grant nos. R21AT009173, R61AT009864, R33AT009864 to T.T.Y.), the National Institutes of Health (RO1 MH129832 to L.S. and UCSF-CTSI UL1TR001872 to T.T.Y.), the National Institute of Mental Health (project no. R01MH125850 to M.D.S. and R01MH085734 to T.T.Y.), the Rebecca L. Cooper Foundation Fellowship (A.Z.), the Rubicon award from the Dutch NOW (grant no. 452020227 to L.K.M.H.), the University of Melbourne Dame Kate Campbell fellowship (L.S.), the UCSF Research Evaluation and Allocation Committee (T.T.Y.) and the UCSF Weill Institute for Neurosciences (T.T.Y.). Data from the MR-IMPACT study site were funded by the United Kingdom Medical Research Council (G0802226) and undertaken at the University of Cambridge. The funders had no role in study design, data collection and analysis, decision to publish or preparation of the manuscript. This research was also supported by The University of Melbourne's Research Computing Services and the Petascale Campus Initiative.

Author contributions

N.Y.T., A.Z., R.F.H.C. and A.R. contributed to the conception and design of the study. N.Y.T., A.Z., R.F.H.C. and A.R. conducted the neuroimaging and statistical analyses with contributions from Y.E.T., C.G.C., C.G.D., I.H.G., B.J.H., T.C.H., A.J.J., J.S.K., Y.L., A.O., J.Q., M.D.S., A.N.S., J.S., D.W. and T.T.Y. contributed data. S.G., X.M. and X.Y. assisted with data collation. N.Y.T., A.Z., R.F.H.C., A.R., L.K.M.H. and L.S. contributed to the writing of the manuscript with input and valuable revision from all authors.

Competing interests

The authors declare no competing interests.

Additional information

Supplementary information The online version contains supplementary material available at https://doi.org/10.1038/s44220-024-00309-y.

Correspondence and requests for materials should be addressed to Andrew Zalesky.

Peer review information *Nature Mental Health* thanks Deanna Barch, Mingrui Xia and the other, anonymous, reviewer(s) for their contribution to the peer review of this work.

Reprints and permissions information is available at www.nature.com/reprints.

Publisher's note Springer Nature remains neutral with regard to jurisdictional claims in published maps and institutional affiliations.

[1]Systems Lab, Department of Psychiatry, Melbourne Medical School, The University of Melbourne, Melbourne, Victoria, Australia. [2]Orygen, Melbourne, Victoria, Australia. [3]Centre for Youth Mental Health, The University of Melbourne, Melbourne, Victoria, Australia. [4]Discipline of Psychiatry and Mental Health, University of New South Wales, Randwick, New South Wales, Australia. [5]Department of Biomedical Sciences, Florida State University, Tallahassee, FL, USA. [6]Department of Psychiatry, The University of Melbourne, Parkville, Victoria, Australia. [7]Department of Biomedical Engineering, Faculty of Engineering and Information Technology, The University of Melbourne, Melbourne, Victoria, Australia. [8]Contemplative Studies Centre, Melbourne School of Psychological Sciences, The University of Melbourne, Melbourne, Victoria, Australia. [9]Department of Psychology, Stanford University, Stanford, CA, USA. [10]Department of Psychology, University of California, Los Angeles, CA, USA. [11]Department of Psychiatry, Columbia University, New York, NY, USA. [12]Division of Child and Adolescent Psychiatry, New York State Psychiatric Institute, New York, NY, USA. [13]School of Artificial Intelligence, Beijing University of Posts and Telecommunications, Beijing, China. [14]Mental Health Center and Laboratory of Psychiatry, West China Hospital of Sichuan University, Chengdu, China. [15]Center for Neural Basis of Cognition, University of Pittsburgh, Pittsburgh, PA, USA. [16]Center for Neuroscience, University of Pittsburgh, Pittsburgh, PA, USA. [17]Key Laboratory of Cognition and Personality (SWU), Ministry of Education, Chongqing, China. [18]Department of Psychology, Southwest University, Chongqing, China. [19]Meditation Research Program, Department of Psychiatry, Massachusetts General Hospital, Harvard Medical School, Boston, MA, USA. [20]VA San Diego Healthcare System, San Diego, CA, USA. [21]Department of Psychiatry, University of California San Diego, La Jolla, CA, USA. [22]Department of Psychiatry, Herchel Smith Building for Brain and Mind Sciences, University of Cambridge, Cambridge, UK. [23]Cambridgeshire and Peterborough NHS Foundation Trust, Cambridge, UK. [24]Department of Psychiatry and Behavioral Sciences, Division of Child and Adolescent Psychiatry, Weill Institute for Neurosciences, University of California, San Francisco, CA, USA. [25]These authors contributed equally: Robin F. H. Cash, Andrew Zalesky. ✉e-mail: azalesky@unimelb.edu.au

https://doi.org/10.1038/s44220-024-00309-y

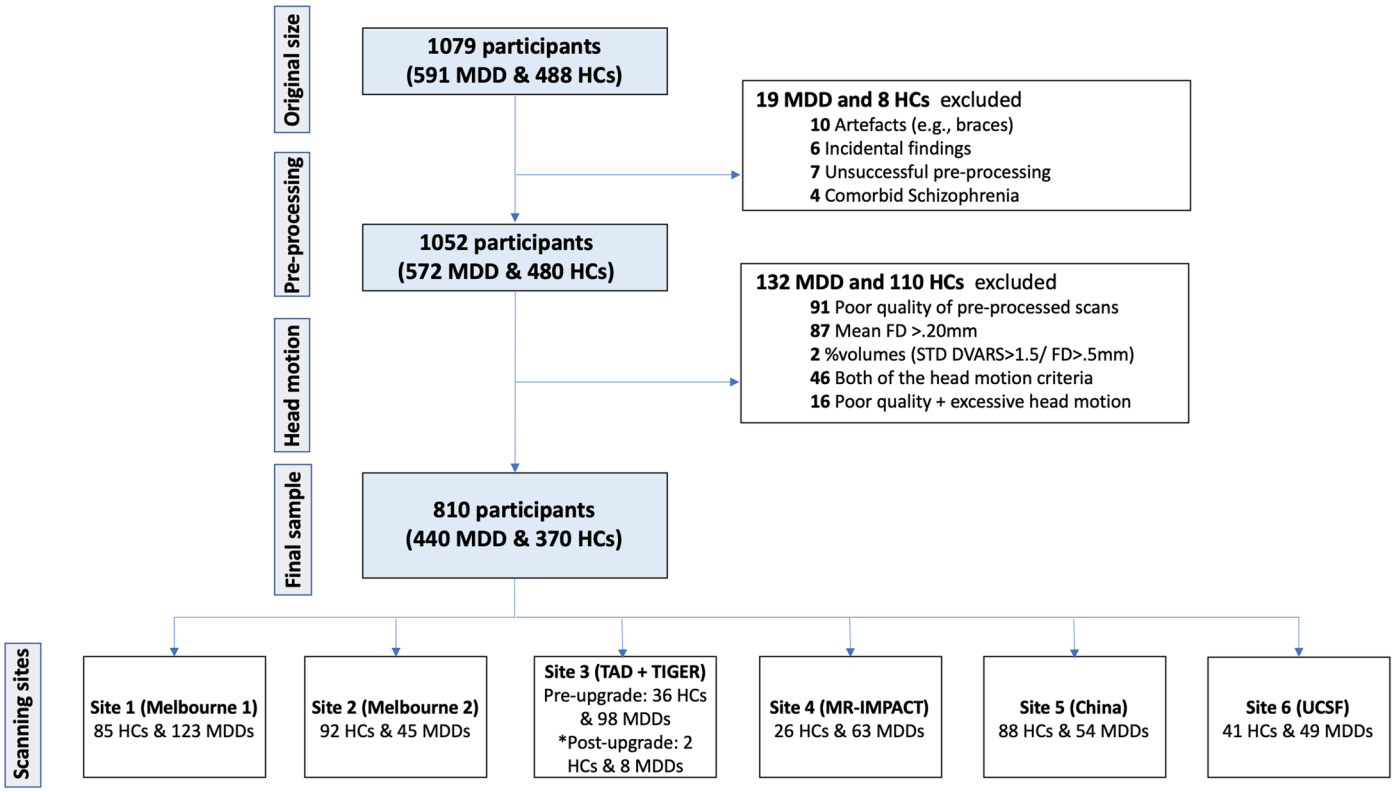

Extended Data Fig. 1 | Participant exclusion flowchart. Flowchart outlining the number of participants excluded and the reason for exclusion following each stage of processing. HC = healthy control; MDD = major depressive disorder.

nature portfolio

Corresponding author(s): Andrew Zalesky

Last updated by author(s): Aug 4, 2024

Reporting Summary

Nature Portfolio wishes to improve the reproducibility of the work that we publish. This form provides structure for consistency and transparency in reporting. For further information on Nature Portfolio policies, see our Editorial Policies and the Editorial Policy Checklist.

Statistics

For all statistical analyses, confirm that the following items are present in the figure legend, table legend, main text, or Methods section.

n/a	Confirmed	
☐	☒	The exact sample size (*n*) for each experimental group/condition, given as a discrete number and unit of measurement
☐	☒	A statement on whether measurements were taken from distinct samples or whether the same sample was measured repeatedly
☐	☒	The statistical test(s) used AND whether they are one- or two-sided *Only common tests should be described solely by name; describe more complex techniques in the Methods section.*
☐	☒	A description of all covariates tested
☐	☒	A description of any assumptions or corrections, such as tests of normality and adjustment for multiple comparisons
☐	☒	A full description of the statistical parameters including central tendency (e.g. means) or other basic estimates (e.g. regression coefficient) AND variation (e.g. standard deviation) or associated estimates of uncertainty (e.g. confidence intervals)
☐	☒	For null hypothesis testing, the test statistic (e.g. *F*, *t*, *r*) with confidence intervals, effect sizes, degrees of freedom and *P* value noted *Give P values as exact values whenever suitable.*
☒	☐	For Bayesian analysis, information on the choice of priors and Markov chain Monte Carlo settings
☒	☐	For hierarchical and complex designs, identification of the appropriate level for tests and full reporting of outcomes
☐	☒	Estimates of effect sizes (e.g. Cohen's *d*, Pearson's *r*), indicating how they were calculated

Our web collection on statistics for biologists contains articles on many of the points above.

Software and code

Policy information about availability of computer code

Data collection	No software was used for data collection.
Data analysis	All the neuroimaging preprocessing and analyses conducted in this study involved the use of publicly available toolboxes and resources. This included the fMRIPrep version 23.0.1 (accessible at https://fmriprep.org/en/stable/installation.html), the combined Schaefer 400 cortical and Melbourne Subcortex Atlas (accessible at https://github.com/yetianmed/subcortex/tree/master/Group-Parcellation/3T/Cortex-Subcortex), NBS MATLAB toolbox version 1.2 (accessible at https://www.nitrc.org/projects/nbs/) and ComBat Harmonization package (https://github.com/Jfortin1/ComBatHarmonization). All cortical renderings were generated using the GUI-based toolbox BrainNet Viewer version 1.7 (https://www.nitrc.org/projects/bnv) via MATLAB. For predictive analyses, dimension reduction via PCA was performed using the pca function in MATLAB version R2021a. This was followed by classification and regression analyses performed using the fitclinear and fitrlinear MATLAB functions, respectively.

For manuscripts utilizing custom algorithms or software that are central to the research but not yet described in published literature, software must be made available to editors and reviewers. We strongly encourage code deposition in a community repository (e.g. GitHub). See the Nature Portfolio guidelines for submitting code & software for further information.

Data

Policy information about availability of data

All manuscripts must include a data availability statement. This statement should provide the following information, where applicable:

- Accession codes, unique identifiers, or web links for publicly available datasets
- A description of any restrictions on data availability
- For clinical datasets or third party data, please ensure that the statement adheres to our policy

The current study did not involve the use of publicly available datasets, but de-identified data from 7 previously published datasets collected by 6 research groups across 4 counties. Data may be made available upon reasonable request at the discretion of each respective principal investigator. Data sharing will be subject to the policies and procedures of the institution where each dataset was collected. Principal investigators from sites that provided data used in this study include C.G.D. (Site 1 and 2), I.H.G. (Site 3 TAD dataset), B.J.H. (Site 1 and 2), T.C.H. (Site 3 TIGER dataset), J.Q. (Site 5), J.S. (Site 4), and T.T.Y. (Site 6). Please direct all data requests to N.Y.T. at ngayant@student.unimelb.edu.au.

Human research participants

Policy information about studies involving human research participants and Sex and Gender in Research.

Reporting on sex and gender	The term sex was used consistently in the study to indicate biological attribute. Sex information for participants was based self-report. The current sample involved 528 females and 282 males. To investigate potential sex interaction effects, supplementary analysis with the additional inclusion of sex by diagnosis interaction term was conducted. Sex was also included as a covariate in all main neuroimaging analyses.
Population characteristics	Structural and resting-state fMRI data were collated across 7 existing cohorts scanned at 6 international sites, yielding a combined sample of 810 young participants aged 12-25 years (528 females and 282 males). Brain imaging was performed across 6 sites in Australia, China, the UK, and the US. The final sample comprised 488 young individuals with a confirmed current diagnosis of major depressive disorder (mean age = 18.39 years) and 587 healthy comparison individuals (mean age = 20.12 years). Diagnostic assessments varied across cohorts and consisted of either the Kiddie Schedule for Affective Disorders and Schizophrenia–Present and Lifetime (K-SADS-PL) or the Structured Clinical Interview (SCID) based on the DSM-IV diagnostic criteria.
Recruitment	Cohorts for inclusion in the planned mega-analysis were identified based on database searches for journal articles that investigated resting-state functional connectivity in youth MDD (irrespective of the inclusion of a healthy comparison group), published until February 2022. Corresponding authors of appropriate studies were contacted between May 2022 and August 2022 and invited to contribute data to the mega-analysis. A total of 27 datasets were identified and 6 groups agreed to provide the required neuroimaging data. Beyond non-response, reasons for nonparticipation included departmental- and ethics- related restrictions on data sharing. As such, the presence of self-selection bias is unlikely.
Ethics oversight	This study was approved by the University of Melbourne Human Research Ethics Committees (2022-24565-31548-4).

Note that full information on the approval of the study protocol must also be provided in the manuscript.

Field-specific reporting

Please select the one below that is the best fit for your research. If you are not sure, read the appropriate sections before making your selection.

☒ Life sciences ☐ Behavioural & social sciences ☐ Ecological, evolutionary & environmental sciences

For a reference copy of the document with all sections, see nature.com/documents/nr-reporting-summary-flat.pdf

Life sciences study design

All studies must disclose on these points even when the disclosure is negative.

Sample size	Cohorts for inclusion in the planned mega-analysis were identified based on database searches for journal articles that investigated resting-state functional connectivity in youth MDD (irrespective of the inclusion of a healthy comparison group), published until February 2022. Corresponding authors of appropriate studies were contacted between May 2022 and August 2022 and invited to contribute data to the mega-analysis. A total of 27 datasets were identified and 6 groups agreed to provide the required neuroimaging data. Beyond non-response, reasons for nonparticipation included departmental- and ethics- related restrictions on data sharing. The final sample following quality control comprised 440 youths with major depressive disorder and 370 healthy comparison individuals aged between 12 and 25 years.

Data exclusions	An initial sample of 1075 young participants were collated from 6 international sites. The number of participants excluded and the reason for exclusion following each stage of processing is outlined in detail in Extended Data Figure 1. Specifically, a total of 269 individuals were excluded due to incidental/ pathological findings (n = 6), the presence of artefacts (e.g., braces; n = 10) or a comorbid schizophrenia diagnosis (n = 4), excessive head motions (n = 151), unsuccessful pre-processing (n = 7), or poor quality scans (e.g., poor anatomical and functional registration, poor field of view; n = 91). This yielded a final sample of 810 youth participants (440 youths with major depressive disorder and 370 healthy comparison individuals).
Replication	A leave-one-site-out cross-validation machine learning method was leveraged to investigate generalizability of the predictive models to unseen datasets acquired at distinct study sites. Specifically, support vector machines (SVM) were trained to predict individual diagnostic status and depressive symptom score (i.e., site-regressed MADRS) based on functional connectivity profiles. Data was first partitioned into training and test sets such that N-1 sites were used for model training, whilst the remaining site was reserved as the test set (i.e., a total of 5 and 6 iterations for classification and regression analysis, respectively). Our predictive models could distinguish youth with MDD from healthy comparison individuals with an average accuracy of 73% (an overall area under the curve [AUC] of receiver operating characteristic [ROC] of 73.1% across all held-out test sets), as well as significantly predict symptom severity with an overall r value of .14 (p =.008) across all leave-one-site-out cross-validation models, supporting the overall generalizability of the findings.
Randomization	Randomization is not applicable here as none of the participants were allocated to experimental groups for the current study with all available resting-state fMRI data for youths with major depressive disorder and healthy comparison individuals being included in all analyses.
Blinding	As described above, none of the participants was allocated to experimental groups for all analyses and therefore, blinding is not applicable to the current study.

Reporting for specific materials, systems and methods

We require information from authors about some types of materials, experimental systems and methods used in many studies. Here, indicate whether each material, system or method listed is relevant to your study. If you are not sure if a list item applies to your research, read the appropriate section before selecting a response.

Materials & experimental systems

n/a	Involved in the study
☒	☐ Antibodies
☒	☐ Eukaryotic cell lines
☒	☐ Palaeontology and archaeology
☒	☐ Animals and other organisms
☒	☐ Clinical data
☒	☐ Dual use research of concern

Methods

n/a	Involved in the study
☒	☐ ChIP-seq
☒	☐ Flow cytometry
☐	☒ MRI-based neuroimaging

Magnetic resonance imaging

Experimental design

Design type	Structural and resting-state functional MRI
Design specifications	No experimental design was involved.
Behavioral performance measures	No behavioral performance measures were collected during the resting-state scan.

Acquisition

Imaging type(s)	T1-weighted and resting-state functional MRI
Field strength	3T
Sequence & imaging parameters	Structural MRI of brain anatomy (T1 images) and unprocessed resting-state fMRI images were collated across 7 existing cohorts scanned at 6 international sites. MRI acquisition parameters for each individual site are detailed in Supplementary Table 4.
Area of acquisition	Whole brain

Diffusion MRI ☐ Used ☒ Not used

Preprocessing

Preprocessing software	Pre-processing was performed using fMRIPrep version 23.0.1, which was based on Nipype 1.8.5.

Normalization	Nonlinear volume-based registration
Normalization template	Registration and normalization of images to FSL's Montreal Neurological Institute (MNI) ICBM 152 non-linear 6th Generation Asymmetric Average Brain Stereotaxic Registration Model (MNI152NLin6Asym) were conducted.
Noise and artifact removal	Output reports of all pre-processed scans were individually inspected and exclusion of scans secondary to artefacts (e.g., braces), pathologies/incidental findings, unsuccessful pre-processing, and/or poor quality of pre-processed scans (e.g., poor anatomical and functional registration, poor field of view) was established by consensus among investigators, N.Y.T., R.F.H.C., and A.Z.. To ensure that current findings were unlikely to be biased by potential confounding influences of head motion, individuals with a mean framewise displacement (FD) >2mm or standardized DVARS (i.e., the derivative of root mean square [RMS] variance over voxels) >1.5 and/or FD >.5mm for more than 20% of the volumes (i.e., outlier volumes) were excluded. The mean FD, standardized DVARS, and RMSD (root mean square deviation; i.e., a quantification of the estimated relative [frame-to-frame] bulk head motion) values and percentage of outlier volumes were also included as an additional covariate in supplementary analyses. For further head motion artifact removal, additional supplementary analyses, adopting a more stringent exclusion criteria of mean FD >1.5mm and 20% outlier volumes, were conducted. Following exclusion, the 24 head motion parameters and their derivatives, as well as signals from white matter, cerebrospinal fluid, and global signal were regressed from the processed fMRI time series. Regressors from discrete cosine transformation (DCT) basis functions were also included for high-pass filtering. Global signal regression (GSR) was used to further alleviate head motion, given that the population studied may be susceptible to motion artifacts. Supplementary analyses without the application of GSR were also conducted.
Volume censoring	No volume censoring was conducted.

Statistical modeling & inference

Model type and settings	The network-based statistic (NBS) was used to test for between-group differences in functional connectivity. Specifically, using the functional matrices, the NBS statistically localized subnetworks of connections with increased or decreased connectivity in the MDD group, compared to the healthy comparison individuals. The NBS was also used to identify connections for which variation in connectivity strength across MDD individuals was associated with variation in symptom severity. An edge-forming threshold of t >3.5 was used. Family-wise error correction at p <.05 was deemed statistically significant and 5000 permutations were generated to estimate the null distribution for the NBS. Support vector machines (SVM) were trained to predict individual diagnostic status and depressive symptom score based on functional connectivity profiles using leave-one-site-out cross validation. Specifically, data was first partitioned into training and test sets such that N-1 sites were used for model training, whilst the remaining site was reserved as the test set. Functional connectivity data was summarized in the form of a matrix X of dimensions M× 102,831 matrix, where M is the number of individuals comprising the training set and 102,831 is the number of unique functional connections. To reduce the dimensionality of the functional connectivity space, principal component analysis (PCA) was applied to X, yielding a 102,831×M-1 matrix of principal component coefficients, C, and a corresponding M×M-1 matrix of principal component scores, S. The PCA decomposition could be represented as $X=SC'$. The SVM was trained using the top 60 principal component scores stored in S.
Effect(s) tested	Not applicable.

Specify type of analysis: ☒ Whole brain ☐ ROI-based ☐ Both

Statistic type for inference (See Eklund et al. 2016)	An edge-forming threshold of t >3.5 was used. Family-wise error correction at p <.05 was deemed statistically significant and 5000 permutations were generated to estimate the null distribution for the NBS.
Correction	All NBS analyses controlled for family wise error.

Models & analysis

n/a	Involved in the study
☐	☒ Functional and/or effective connectivity
☒	☐ Graph analysis
☐	☒ Multivariate modeling or predictive analysis

Functional and/or effective connectivity	Pearson correlation coefficient was used to compute functional connectivity.
Multivariate modeling and predictive analysis	Support vector machines (SVM) were trained to predict individual diagnostic status and depressive symptom score based on functional connectivity profiles using leave-one-site-out cross validation. Specifically, data was first partitioned into training and test sets such that N-1 sites were used for model training, whilst the remaining site was reserved as the test set. Functional connectivity data was summarized in the form of a matrix X of dimensions M× 102,831 matrix, where M is the number of individuals comprising the training set and 102,831 is the number of unique functional connections. Principal components analysis (PCA) was performed on the training data to reduce the dimensionality of the functional connectivity matrices and alleviate the risk of overfitting. SVM models were trained on the resulting principal component scores. The test data (i.e., held-out site) were projected on the principal components and resulting scores were used to derive predictions. PCA was performed separately for each training fold. Given the stochastic nature of the

model fitting algorithm (stochastic gradient descent), the entire model fitting and evaluation process was repeated 100 times and model performance was averaged across the 100 iterations, unless otherwise stated.